UNIVERSITÄT DUISBURG ESSEN

Offen im Denken

Final Report for:

"Weitergehende Untersuchungen zum Fouling von Ultrafiltrationsmembranen bei der Aufbereitung von ölhaltigen Wässern" (W-UFO I)

April 2018 - July 2019

Team:

University of Duisburg-Essen
Faculty of Engineering
Department of Mechanical Engineering and Process Engineering
Chair of Mechanical Process Engineering / Water Technology

Lotharstr. 1

47057 Duisburg

www.uni-due.de/wassertechnik/

Prof. Dr.-Ing. Stefan Panglisch (Project PI)
Telefon: 0203 379 -3477

stefan.panglisch@uni-due.de

M.Sc. Hasan Idrees
Telefon: 0203 379 -3477

hasan.idrees@uni-due.de

Projektförderung durch die

Willy-Hager Stiftung
c/o Technische Universität Kaiserslautern
Paul-Ehrlich-Straße 14
67663 Kaiserslautern

Ansprechpartnerin:
Prof. Dr.-Ing. Heidrun Steinmetz

Project period: April 2018 to July 2019

Contents

1 Abstract

One of the most serious environmental pollutants in the last years is oily wastewater, mainly produced water from oil and gas industries. That water has to be treated properly to match the environmental standards before discharged into the surrounding environment. Dead end membrane filtration is considered a potential treatment technique of oily wastewater, especially as polishing step when the water contains mainly fine oil droplets of average diameter <10 µm in low concentration. Nevertheless, one main drawback of this method is the fast and significant decay in membrane performance due to membrane fouling. To overcome this issue, it is essential to gather a comprehensive understanding about fouling behavior and all influencing parameters.

This project has focused on investigating the influence of oil droplet size and size distribution of coarse oil without any further ingredients like surfactants on the membrane fouling mechanisms during filtration of low concentrated oily wastewater (5 ppm). In order to produce a droplet size as small as possible high-pressure homogenizer with pressures up to 1,900 bar were used. Because of the high mechanical stress applied it can be assumed that smaller droplet size cannot occur at least without surfactants. Dead-end filtration experiments were carried out using polyethersulfone and ceramic microfiltration (MF) and ultrafiltration (UF) flat sheet membranes exhibiting different average barrier pore diameters ranging between 0.02 and 1.2 µm. The filtration experiments were alternatively performed at constant pressure or constant filtration rate.

The results have emphasized the significant impact of oil droplet size and membrane average barrier pore diameter on the observed fouling behavior and mechanisms. The fouling mechanisms were investigated using classical pore blocking filtration models. The chronological evolution of membrane fouling mechanisms showed that the influence of oil droplet size was more pronounced for membranes of larger or comparable pore size than the oil droplet size (in the present case MF membranes). In this case standard pore blocking followed by intermediate blocking then cake filtration was observed. For membranes with smaller pore size (in the present case UF membranes) intermediate pore blocking was initially dominant

and followed by cake layer formation. Furthermore, investigation of the cross-section morphology of the fouled membranes using scanning electron microscope showed that oil droplets were trapped inside membranes with larger pore size and coated the internal structure, whereas most of oil droplets were retained on top of more dense membranes and no oil was seen deeply within the internal porous structure. This indicates that using membranes with pore sizes significantly smaller than oil droplets might cause much less fouling. Accordingly, it is highly recommended to analyze oily feeds in terms of droplet size distribution to choose the most suitable membrane, i.e., the one with pores smaller than oil droplets, to avoid internal fouling. Addition of salts was found to disturbs the stability of oil nano-emulsions and resulting in bigger oil droplets, and consequently, oil droplet size distributions with bigger droplets are highly expected in case of real saline produced water. Subsequently, oily feeds caused less membrane fouling.

Further on, performing experiments at high initial pressure in case of constant pressure experiments have led to intensive internal fouling and severe decay in membrane performance. In contrast increasing TMP at later filtration periods was observed to have less detrimental impact on membrane performance, as in case of constant flux experiments. This effect will be addressed more detailed in future work, e.g., identification of maximum critical pressure, as well as maximum flow rate, that can be applied without causing initial severe fouling to reduce fouling.

Moreover, a set of membrane cleaning tests were conducted using 0.45 µm ceramic membranes. Many cleaning agents and protocols were applied to find out the most effective procedure. Tests indicated that rinsing of membranes with sodium hydroxide (NaOH) at pH=14 and 100 °C for 60 min tend to yield the highest permeability recovery of 98%.

2 Introduction

Huge amounts of hazardous oily wastewater are annually produced from oil and gas industry. This oil-contaminated water, also known as produced water (PW), is either generated naturally, i.e. water existing within the geological structure of wells or because of water injection required for increasing the well performance, so-called “flow back water”. For instance, an average of 300 million barrels of produced water were produced per day in 2017 [1]. Oily wastewater is also produced

from other sources, e.g. oil refineries, petrochemical and metal industries, oil transport facilities, gas and car wash stations as well as restaurants. The composition of PW differs depending on the geographical location of the well [2]. PW is mainly composed of dissolved and dispersed oil components, dissolved minerals, production chemicals (e.g. corrosion and scale inhibitors), produced solids (e.g. clays and waxes), as well as dissolved gases (e.g. CO_2, O_2, H_2S) [3, 4]. The oil content in PW comprises four organic compounds, i.e. aliphatic hydrocarbons, phenols, carboxylic acids and polycyclic aromatic hydrocarbons [5, 6]. PW is found to be slightly acidic with oil content in the range of 2 – 2,000 mg/L, total suspended solids of 1 - 1,000 mg/L and total dissolved solids of 1,000 - 400,000 mg/L [7, 8]. Recent studies reveal that the global production of PW will continue to grow significantly because of oil and gas wells aging that is always accompanied by increasing in the volumes of produced water [1]. Moreover, the global oil/water ratio is expected to reach 1:12 by 2025, in comparison with 1:3 in 2011 [4]. In parallel, more stringent regulations for oily wastewater discharge have been made. In January 2007, the Convention for the Protection of the Marine Environment of the North-East Atlantic by Oslo and Paris Commissions have set a daily limit of 30 mg/L oil concentration at oily-wastewater disposal. Concurrently, the potential of reusing produced water as fresh water is gaining more attention and interest in water-stress oil-producing countries, therefore, efficient treatment methods are required [9]. Critical reviews have surveyed all reported technologies for oily-wastewater treatment and concluded that membrane-based separation processes, especially UF, are promising because of high water recovery, simplicity, small footprint and ease to be integrated into currently established treatment plants [3, 4, 7, 8, 10]. Moreover, in combination with other methods, more than 3,000 polymeric UF / MF and more than 75 inorganic / ceramic membrane treatment units have been installed worldwide [11]. Nevertheless, the high fouling tendency of polymeric UF membranes by oily-contaminated water is still one of major issue. The retention behavior, as well as fouling mechanisms, are always complicated in such applications, and are highly influenced by the operating conditions.

3 Project objective

The ultimate objective of W-UFO research project series is to establish an efficient membrane-based treatment method for produced water feeds using polymeric ultrafiltration (UF) membranes. This method is targeted as a polishing step in the treatment of oily wastewater effluents containing oil substances (oil in water concentration below 20 mg/L), i.e., produced water after primary and secondary processes, with an average oil droplet size smaller than 1 µm. To achieve that, it is essential to gather a deep understanding of UF membrane performance and fouling mechanisms during filtration of different oil-contaminated feeds, at different operating conditions. The project plan is divided into four subprojects: W-UFO I – IV, one-year duration for each subproject, which gives the advantage of revising as well as modifying views and targets of the project according to the outputs and knowledge gained by each subproject. W-UFO I (that is the subject of this report) aims at studying the influence of oil droplet size distribution on fouling mechanisms and coalescence phenomena, as well as the influence of salts in the feed solution on the stability of nano-emulsions and the fouling mechanisms. W-UFO II will focus on the impact of using surfactants and co-surfactants on the stability of nano-emulsions and droplet size distribution, UF membrane performance and fouling mechanisms. W-UFO III will be devoted to quantifying the dissolved oil portions in oily-wastewater and studying their influence on UF membrane performance and fouling behavior. In addition, an investigation of the possibility of enhancing the filtration performance via dosing of powdered activated carbon or flocculants will be conducted. W-UFO IV will evaluate the outputs of the aforementioned three subprojects, along with the adaptation of the operating parameters (e.g., membrane flux, filtration mode, backwash frequencies), and/or the membrane surface properties. Semi-pilot scale experiments using real produced water may be also included.

4 Project progress summary

- All work packages were executed as planned in our proposal. During the project execution and based on experiments outputs, two parameters were however altered from the original plan:
    - Nano-emulsions with oil droplets in size range of 50 – 2,000 nm, instead of 5 to 200 nm (as planned) were prepared. First reason was

to simulate a real produced water sample got from a crude oil and natural gas producer, Germany, and this sample we analyzed for the droplet size distribution (see **Appendix**). Second reason was to match the droplet size in this way that droplets are mostly smaller or in the range of the pore size of MF and at the same time mostly larger than the pores of UF.

- Polymeric membranes were also employed, besides ceramic membranes (as planned) for filtration experiments at constant flux and those at constant pressure conditions. Using cost-efficient polymeric membranes was more feasible for using new membrane for each experiment, which was a necessity since ceramic membranes suffered from irreversible fouling that could not be restored completely by any tested cleaning agent. In addition, polymeric membranes had an advantage of ease internal morphological testing using scanning electron microscope.

- Because of unexpected pump failure and other technical issues, a new lab-scale filtration unit was needed, we proposed to use the budget which was supposed to be used for purchasing a temperature controller (Ministat 240w mit Regler „Pilot ONE“) that was proposed in the project. A fully-automated plant was designed and ordered after getting the approval from the project administration. Further technical issues were faced especially with the high-pressure homogenizer which went out of order several times, these all led to a certain delay in project's progress. As a result, an extension of the project lifetime of 4 month was needed to achieve the project target.

- The main scientific outputs were presented in three international scientific conferences:

  - "Euromembrane 2018" in Valencia, Spain
  - "Aachener Membran Kolloquium 2018" in Aachen
  - "IWA Membrane Technology conference 2019 in Toulouse, France

  Furthermore, the project results have been accepted to be presented as oral presentation in three coming international conferences:

  - "Filtech, October 2019" in Cologne, Germany, that also includes a submission of full conference paper,

- "IWA Particle Separation Specialist Conference, November 2019", in Amherst, Massachusetts, USA
- "4th International Conference on Desalination using Membrane Technology, December 2019", Perth, Australia.

Moreover, it is planned to publish one paper in a peer-reviewed journal. The funding by Willy-Hager will be acknowledged in these conferences and scientific paper.

5 Main scientific and technical outputs

5.1 Material and methods

5.1.1 Chemicals

For oil-in-water nano-emulsions preparation, a standard light crude oil (AR-2048, 2.01 wt.% Sulfur) was selected which was procured from Alpha Resources LLC, USA; to ensure a reproducible source of oil. As listed in **Table 1**, the content of polycyclic aromatic hydrocarbon (PAH) components in the crude oil has been analyzed by the organic analysis department at IWW water center, Mülheim an der Ruhr, using Gas Chromatography – Flame Ionization Detector (GC-FID) according to the US-EPA 16 PAH list, which has the determination limit of 3 mg/L. Pure water (DI) was provided by a reverse osmosis water system (Model: Osmose 190, Denerle, Germany) with a permeate quality (conductivity: ~ 35 µS/cm, dissolved organic carbon content: < 0.2 ppm). Ethanol 96% denatured, purchased from Carl Roth® GmbH (Density: 0.81 g/mL, Molar mass: 46.07 g/mol) was employed for cleaning. Sodium hydroxide (NaOH) acetic acid (CH_3COOH), Sodium chloride (NaCl), Calcium Chloride ($CaCl_2$) and sodium hypochlorite (NaOCl) were obtained from VWR International.

Table 1: Crude oil content of polycyclic aromatic hydrocarbon (PAH) components measured using GC-FID, , according to the USEPA 16 PAH list; <3 means that the value was below the measurement determination limit

PAH components	Concentration in mg/L	PAH components	Concentration in mg/L
Acenaphthen	<3	Acenaphthylen	<3
Dibenz[a,h]anthracen	<3	Anthracen	<3
Fluoranthen	<3	Benzo[a]anthracen	35
Fluoren	<3	Benzo[a]pyren	<3
Indeno[1,2,3-c,d]py-	<3	Benzo[b]fluoranthen	<3
Naphthalin	620	Benzo[ghi]perylen	<3
Phenanthren	150	Benzo[k]fluoranthen	<3
Pyren	3	Chrysen	<3

5.1.2 Artificial Seawater solutions

Artificial seawater salts, Type “Reef Salt”, was purchased from Aquamedic, Germany; the main components of the salts are listed in **Table 2.** To prepare the seawater solutions, 35 g of the salt were solved in DI water.

Table 2: Reef salt artificial seawater salts major elements

Element	Concentration in g/Kg	Element	Concentration in g/Kg
Na	254	Cl	488
Mg	30	SO_4^{-2}	60
Ca	11	HCO_3^-/CO_3^{2-}	4
K	10	H_2O	142

5.1.3 Membranes

A set of MF and UF polymeric and ceramic flat sheet membranes exhibiting different average pore diameters were employed in this study as listed in Table 3. Ceramic membranes were purchased from Tami membranes, France. Polyethersulfone (PES) membranes were supplied by 3M membranes business unit, Pall membranes and inge® water technologies GmbH, Germany. A new polymeric membrane was used for each experiment, while ceramic membranes were used

multiple times after cleaning using NaOH at pH ≈ 14 and 100 °C. All membranes had an active surface area of 13.85 cm².

Table 3: List of membrane samples

Acronym	Average pore diameter or MWCO	Material	Produced by
12F	1.20 µm	PES	3M Mem-
4F	0.40 µm	PES	3M Mem-
1F	0.04 µm	PES	3M Mem-
Inge	0.02 µm	PES	inge BASF
Supor®800 (S800)	0.80 µm	PES	Pall
Supor®450 (S450)	0.45 µm	PES	Pall
Supor®100 (S100)	0.10 µm	PES	Pall
TM 140	1.40 µm	Ceramic	Tami
TM 045	0.45 µm	Ceramic	Tami
TM 050	50 kDa	Ceramic	Tami
TM 015	15 kDa	Ceramic	Tami

5.1.4 Homogenizers

After several tests in previous work, high-pressure homogenizer (HPH) was found to be the best tested way to produce nano-emulsions in terms of small and stable oil droplets of favored size. Oil and water were premixed using stator-rotor mixer.

5.1.4.1 Stator-rotor Mixer

For premixing oil in water nano-emulsions Ultra-Turrax® T25, IKA-Werke GmbH & Co. KG, Germany, a high-speed stator-rotor mixer was employed to produce fine homogenized mixtures before applying high-pressure homogenization. Ultra-Turrax® T25 (**Figure 1**) is designed for dispersing and emulsifying liquid media in batch operation with a maximal energy output of 350 Watt.

Figure 1: Stator-rotor mixer, Ultra-turrax T25 IKA®

5.1.4.2 High pressure homogenizer (HPH)

The HPH **Figure 2** is an inline dispersing machine. It is used for continuous production of superfine emulsions even nano-emulsions. HPH is manufactured by IKA®-Werke GmbH & Co. KG, Germany. HPH consists of a feed emulsion container, a working chamber, a high-pressure piston pump and some accessories such as barometers control valves and high-pressure pipes. During homogenizing, the high pressure was built by the reduction of the cross section in the homogenizing valve. Then the high-turbulent streams were occurred by the releasing of the high pressure in a very narrow adjustable gab of the valve. This high-turbulent can cause a homogenizing.

Figure 2: High Pressure Homogenizer (HPH), manufactured by IKA®-Werke GmbH & Co. KG, Germany

5.1.5 Filtration systems

Filtration tests were conducted using two lab-scale dead-end filtration units. As schematically represented in **Figure 3** and shown in **Figure 4**, the first filtration unit which is a fully-automated filtration system that can be operated at constant pressure (up to 6 bar) and constant flux conditions (constant flow rate up to 2 L/h). It was assembled by convergence B.V. (Netherlands). Filtration experiments were conducted at a constant flux of 240 LMH and the change in transmembrane pressure (TMP), due to fouling, was automatically measured.

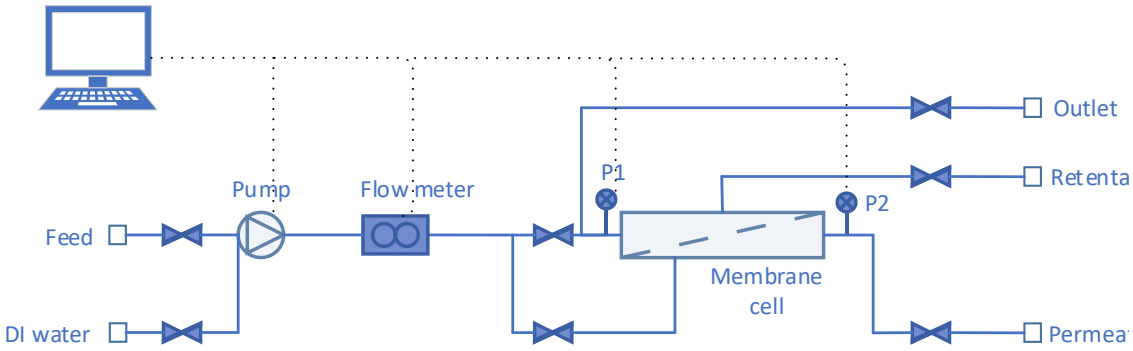

Figure 3: Schematic description of the lab-scale dead-end filtration unit at constant flow rate for flat sheet membranes

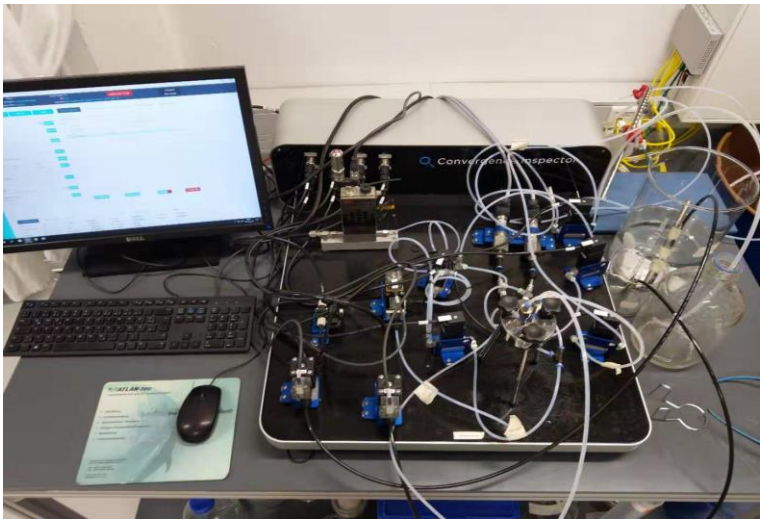

Figure 4: Lab-scale dead-end filtration unit at constant flow rate for flat sheet membranes

For this system a membrane holder supplied by Tami membranes, France with different support layers were employed. For ceramic membrane only spiral rubber support layer was used; For PES membrane the metal screen and paraffin screen

were additionally installed, as shown in **Figure 5.** The system also can be programed to automatically perform the filtration steps and register the measured data like the flow rate and pressure at certain time intervals.

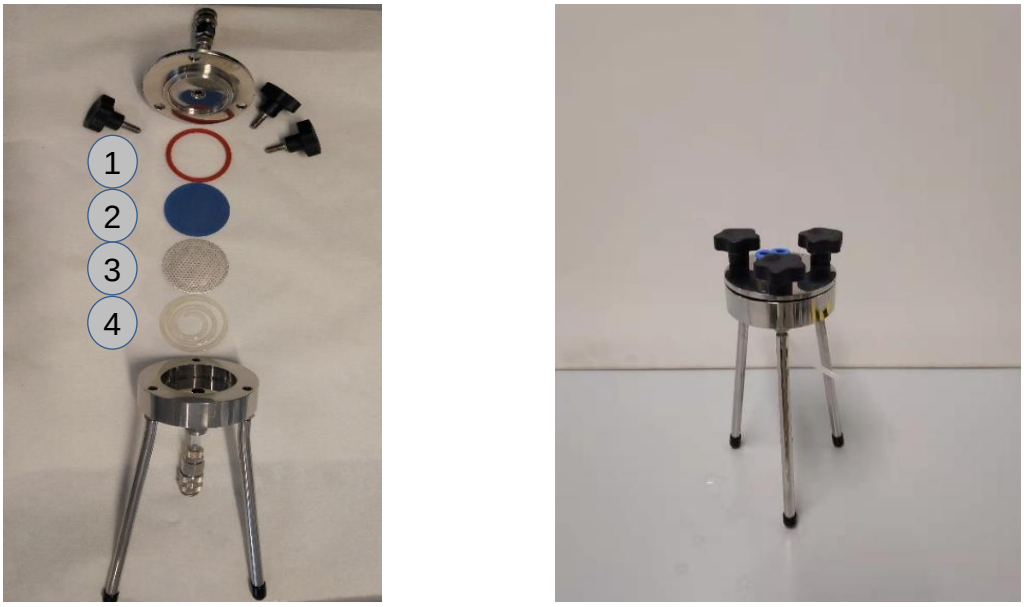

Figure 5: TAMI membrane holder (right) and support layers(Left) which are Sealing (1) 2- Paraffin screen (2) 3- Metal screen (3) Spiral rubber support (4)

The Second filtration unit was operated at constant pressure condition (cf. **Figure 6**). It was designed and assembled to meet ASTM standards (D 4189–95, 2002) for measuring Modified Fouling Index (MFI). The flow rate was determined by weighting the permeate volume at certain time intervals. All filtration experiments were performed at constant room temperature of 22 °C.

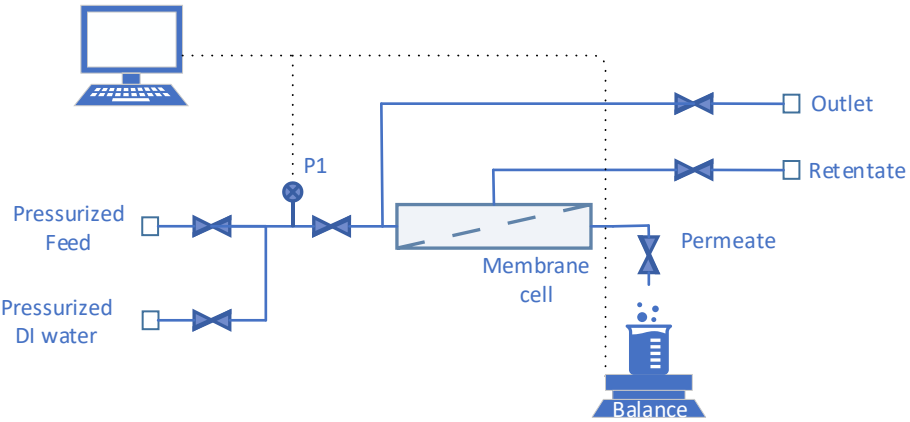

Figure 6: Schematic description of the lab-scale dead-end filtration unit at constant pressure for flat sheet membranes

5.2 Analytics

5.2.1 Droplet size distribution

Oil droplet size distribution was measured using a laser diffraction particle size analyzer, Model: LS 13320, Beckman Coulter, USA, (cf. **Figure 7)**. Which measures the particle size distribution of dispersed materials in the liquid state based on the principle of light scattering, so that the device takes information about droplet size distribution by measuring scattering intensity as a function of the scattering angle, wavelength and polarization of light based on applicable scattering models. The device also incorporates PIDS technology (Polarization Intensity Differential Scattering technology) to provide a dynamic measuring range of 0.017 µm to 2,000 µm.

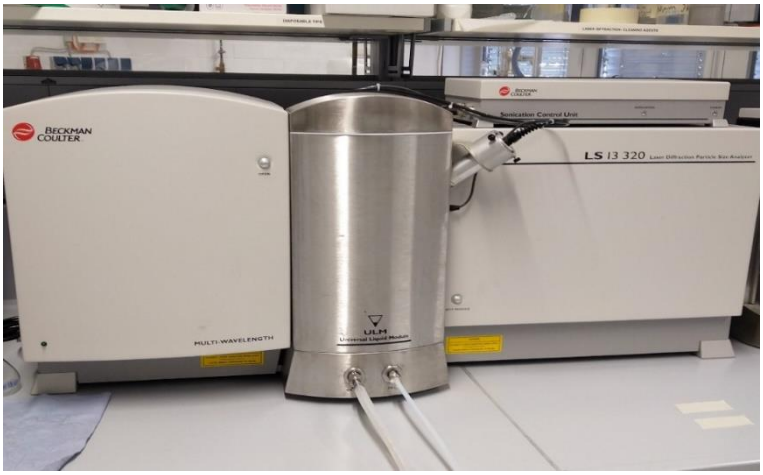

Figure 7: Coulter Beckman LS 13 320 Laser Diffraction particle size analyzer

5.2.2 TOC, Conductivity, pH and turbidity

The oil content of the prepared oily feeds was determined by measuring the total organic carbon (TOC) by TOC-L device (**cf. Figure 8**) which is manufactured by Shmidazu, Japan. The core of the measurement is to combust all organic matter in the samples by heating to 680 °C in an oxygen-rich environment inside combustion tubes filled with platinum catalyst to convert them into carbon dioxide; Generated CO_2 are quantified using an infrared spectrometer. The result of the measurement is an intensity and the device shows the peak area, which have been correlated to TOC content in mg/L. Calibration is performed by measuring the peak area of solutions of potassium hydrogen phthalate with known concentrations.

Calibration has been splitted into two ranges (1 – 10 mg/l; 20 – 100 mg/l) to increase the accuracy of the measurement. Confidence interval was calculated according to Funk et al, 2005 [12], determination limit was calculated according to DIN 32645. **Table 4** indicates the confidence interval and the determination limit for TOC measurement.

Table 4: The confidence interval and the determination limit for TOC measurement with Shimadzu TOC-L device

TOC measurement range	Confidence interval	Determination limit
1 – 10 mg/l	±0.14 mg/l	0.5 mg/l
20 – 100 mg/l	±0.8 mg/l	3 mg/l

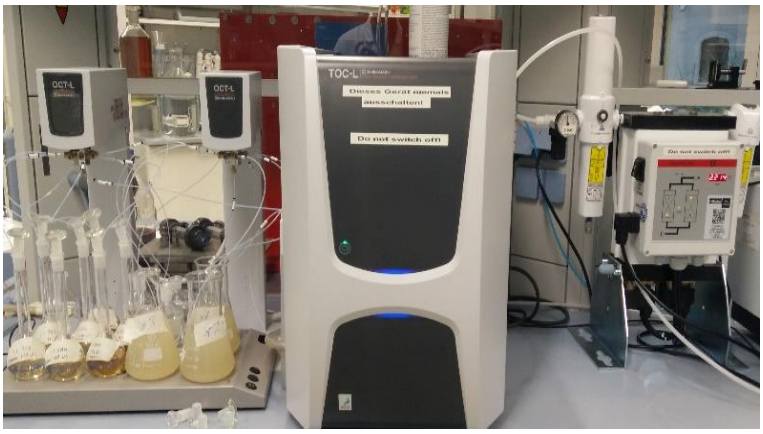

Figure 8: Shimazu TOC-L, TOC measurement device

The pH-value, turbidity and conductivity of feed water and permeate was measured using PH 197i (WTW), Cond 197i (WTW) and NEPHLA turbidity meter (Dr. Lange GmbH & Co. KG), respectively (**cf. Figure 9**).

Figure 9: PH 197i pH meter, WTW (Left), Cond 197i conductivity meter, WTW (middle) and NEPHLA turbidity meter Dr. Lange (right)

5.2.3 Membrane morphology

Scanning Electron Microscope (SEM) (FEI, USA) was used to scan the virgin and fouled membranes' cross section and top surface morphologies at standard high vacuum conditions. Samples were coated with silver using a K-550 sputter coater (Emitech, U.K.). Samples were sputtered for 1.5 min in case of cross section analysis and for 0.5 min for the surface scan. Membranes' morphology was also analyzed by Environmental Scanning Electron Microscope (ESEM) at 60% humidity.

5.2.4 Preparation of oil-in-water nanoemulsions

Chemically identical nano-emulsions of constant oil concentration of 5 ppm exhibiting different droplet size distributions were produced using HPH by applying different operation pressure values, multiple passes and different oil/water volume ratios. To avoid interferences of the emulsifying agents into the fouling mechanisms, the oil nano-emulsions were prepared without using surfactants or emulsifying substances. Crude oil and DI water were mixed at certain oil/water volumetric ratio (1/250, 1/500 or 1/1,000) and initially homogenized by Ultra-Turrax® for one minute to produce so called "Pre-mix". Which was further homogenized by high-pressure homogenizer at different pressures 100 – 1,900 bar to get a nano-emulsion of one emulsification pass. That can further homogenized by applying more passes. Different droplet size distributions nano-emulsions could be achieved by applying different operation pressures and several passes. After each pass, emulsions were cooled down to 35 °C, thereafter another emulsification pass was performed. Since the final target is to simulate the feed of a polishing step in oily wastewater treatment, particles bigger than 10 µm were removed in a fining step, in which a qualitative filter papers can remove the particles bigger than 10 µm (VWR international) were employed (cf. **Figure 10**). However, at the early stage of the study, nano-emulsions' production included no fining, nevertheless, they were employed in this study. Such kind of nano-emulsions is marked with a star over the right side of the emulsion name, e.g. E2*.

Figure 10: Qualitative filter paper (left) and the final product of Nano-emulsion (right)

5.2.5 Filtration experiments

Each flat sheet membrane was cleaned and pre-compacted. Membranes were washed with 50% ethanol solution overnight to eliminate manufacturing residuals and conservatives. Afterwards, membranes were rinsed with pure water overnight to remove the ethanol. Then filtration was performed with pure water at constant pressures, 1 bar for UF and 0.5 bar for MF membranes, for 2 hours as pre-compaction. For the compaction of UF membranes, a pressure vessel was employed to provide the pure water with constant pressure. Because of the high flux of MF membranes during the compaction, a circulatory water system with pump was used, as shown in **Figure 11**. Initial pure water permeability (P_{W0}) was determined by filtering DI water for 15 min before starting oily feed filtration. First, preliminary filtration experiments were carried out at a constant pressure of 2.07 bar to adjust the filtration conditions. The core experiments were conducted at constant operating pressure of 0.5 bar.

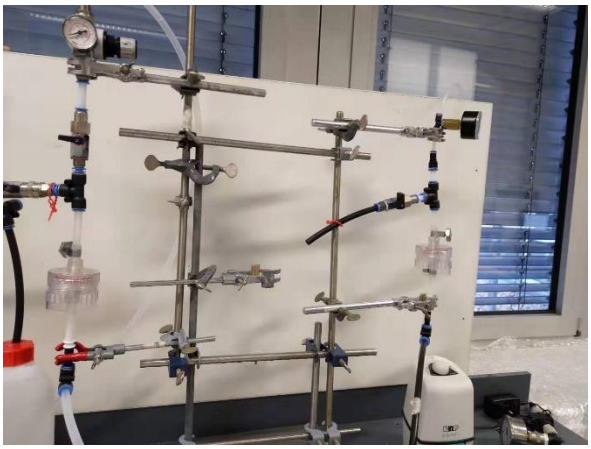

Figure 11: Compaction unit for UF and MF membranes

To ensure the reproducibility of the experiments, either each experiment was repeated once again or when the planned set included high number of experiments, to save time, only a third of the total number of experiments was repeated.

5.2.6 Evaluation of membrane fouling

General speaking, membrane filtration performance can be assessed by determining both filtered volume rate overtime (Q) and transmembrane pressure (TMP) over the filtration progress, from which filtration flux (J), membrane permeability (P) and normalized membrane permeability can be calculated as following:

$$J\ (L/m^2 \cdot \mathrm{h}) = \frac{Filtration\ rate}{membrane\ active\ surface\ area} = \frac{Q\ (L/h)}{A_m\ (m^2)} \quad (1)$$

$$P\ (L/m^2 \cdot \mathrm{h} \cdot \mathrm{bar}) = \frac{J\ (L/m^2 \cdot h)}{TMP\ (bar)} \quad (2)$$

$$Normalized\ permeability = \frac{Permeability}{Pure\ water\ permeability} = \frac{P}{P_{W0}} \quad (3)$$

Filtered media can block the membrane pores causing a decrease in the filtration performance. Membrane fouling stages can be divided into three main stages starting with membrane pore blocking, then cake layer formation and followed by cake layer compression. Pore blocking can be occurred via three main mechanisms. Complete pore blocking assumes that each particle that reaches the membrane surface tend to settle at the entrance of an open pore and close it completely. Intermediate blocking considers the probability of foulant particles to rest on the membrane to form a cake layer or to block a membrane pore entrance. Standard pore blocking assumes that particles might adsorb into the internal wall of the membrane pore causing severe fouling. **Figure 12** shows a schematic description for the main membrane fouling mechanisms. Several mathematical models were introduced and developed to describe membrane fouling in dead-end mode at both constant pressure e.g. [14-17] and constant filtration rate [18, 19] conditions. The main focus was pointed at pore blocking and cake layer formation. Under certain assumptions, Hermia [16] has developed a general equation which can describe the main four blocking mechanisms under dead-end constant pressure filtration conditions:

$$\frac{\mathrm{d}^2 t}{\mathrm{d}v^2} = k\left(\frac{\mathrm{d}t}{\mathrm{d}v}\right)^n \tag{4}$$

in which t is the filtration time, v is the filtrated permeate volume, and K is a dimensionless fouling coefficient for constant pressure filtration. The potential n is the blocking index which depends on the blocking type: n = 2, 1.5, 1, and 0 for complete blocking, standard blocking, intermediate blocking, and cake filtration respectively. Many publications studied the membrane fouling using Hermia equation at dead-end constant pressure filtration using different foulants such as colloidal silica [20], microorganisms [21], natural organic matter (NOM) [22] and wastewater [23]. Grace [18] introduced an equation that can be applied for constant filtration rate conditions:

$$\frac{\mathrm{d}\boldsymbol{TMP}}{\mathrm{d}\boldsymbol{v}} = \boldsymbol{k'}\,\boldsymbol{TMP}^{\boldsymbol{n'}} \tag{5}$$

Iritani and Katagiri [13] has reviewed the major published work on developing mathematical models that describe the four main blocking mechanisms and could finally introduce a method that bases on graphical identification of the blocking mechanisms by fitting the filtration curves with the graphs shown in **Figure 13** in terms of the linearity expressions.

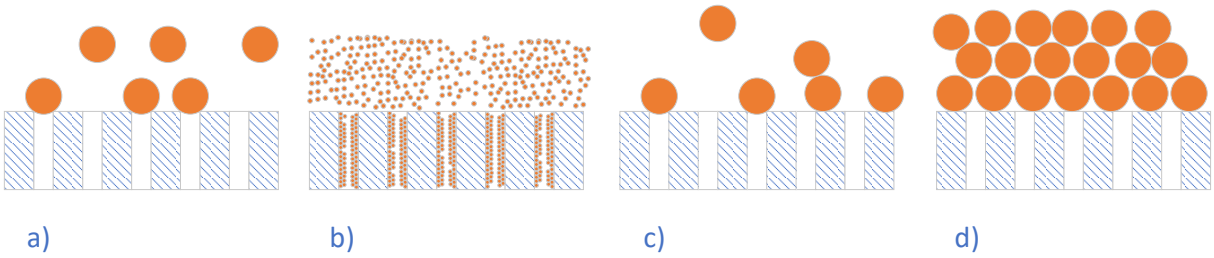

Figure 12: Schematic representation of the four main blocking mechanisms; Complete Blocking (a), Standard blocking (b), Intermediate blocking (c), and Cake filtration(d)

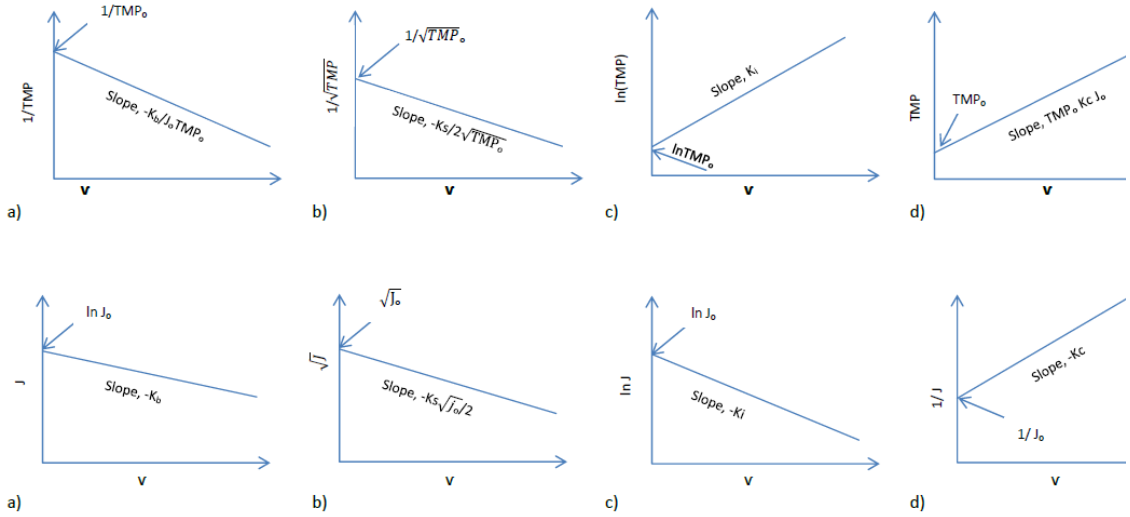

Figure 13: Graphical identification of blocking laws that was finally developed by Iritani and Katagiri [13] for filtration at constant flow rate (top) and constant pressure (bottom) to identify Complete Blocking (a), Standard blocking (b), Intermediate blocking (c), and Cake layer formation (d)

5.2.7 Cleaning of ceramic membranes

These experiments were carried out using TM 045 ceramic membrane, due to their chemical stability in comparison with PES membranes. First, the initial pure water permeability of the membrane was determined. Then, E2 (cf. Chapter 5.3.1) feed was filtered through the membrane at 2.07 bar constant pressure. Afterward, the fouled membrane was backwashed with pure water at 3 bar and then rinsed in the cleaning agent / mixture for 24 h, thereafter the pure water flux was re-measured.

5.3 Results and discussion

5.3.1 Nanoemulsions production

For investigating the influence of oil droplet size distribution on the fouling behavior, three nano-emulsion stock solutions with different oil droplet size distributions were prepared. Objective was to tune droplet size distribution as close as possible to a real produced water[1] but also to match with pore sizes of the used membranes in this way that solutions result with smaller and with larger droplet sizes compared

[1] A produced water sample got from a crude oil and natural gas producer, Germany. The sample was analyzed for droplet size distribution (see **Appendix**)

to the membranes pore size. The preparation procedures of nano-emulsions were adapted via conducting a series of adaptation experiments to find out the influence of each parameter, pressure value, oil/water volume ratios and number of passes. Afterwards, oil nano-emulsion feed solutions were diluted to prepare oily feed solutions of constant oil content (~ 5 mg/L). Using an oil/water volume ratio of 1/250, a series of experiments were conducted applying emulsification pressure values of 500, 1,000, 1,500 and 1,900 bar. The results showed that the produced nano-emulsions has a bi-modal differential volume droplet size distribution, where one main peak is always smaller than 1 µm and a secondary peak is bigger than 1 µm. Results also revealed that high emulsification pressure values were required to produce nano-emulsions exhibiting high portions of oil droplets smaller than 1 µm (cf. **Figure 14**).

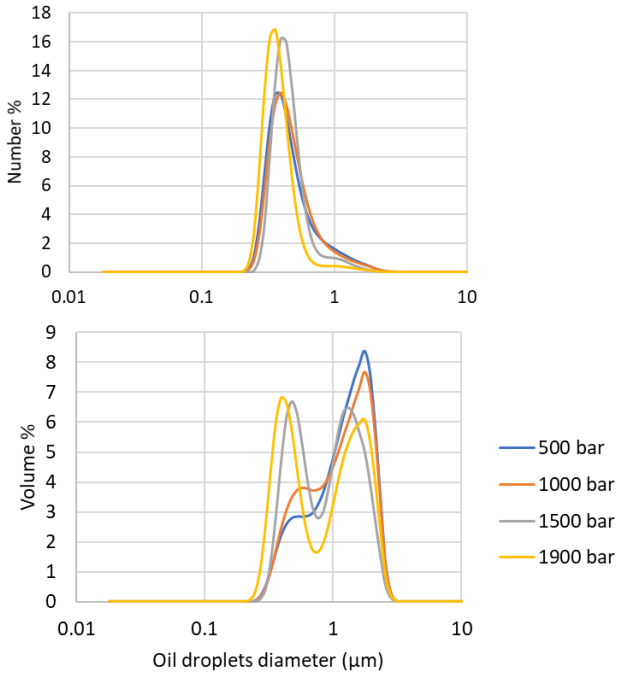

Figure 14: Droplet size distribution of oil nano-emulsions produced at emulsification pressure of 500, 1,000, 1,500 and 1,900 bar using fixed oil/water volume ratio of 1/250

Another series of experiments was carried out, at fixed emulsification pressure of 1,900 bar pressure, in order to investigate the influence of multiple homogenization passes on the oil droplet size. Multiple emulsification passes, up to eight times, were tested. As revealed in **Figure 15**, the intensity of secondary peak was able to be reduced by applying more passes, such that it was eliminated after eight

passes; no further substantial changes were noticed by applying more passes. Furthermore, the number of passes, required to eliminate the secondary peak, was possible to be decreased to 4 passes upon reducing the oil/water ratio to 1/1,000 (cf. **Figure 16** and **Figure 17**).

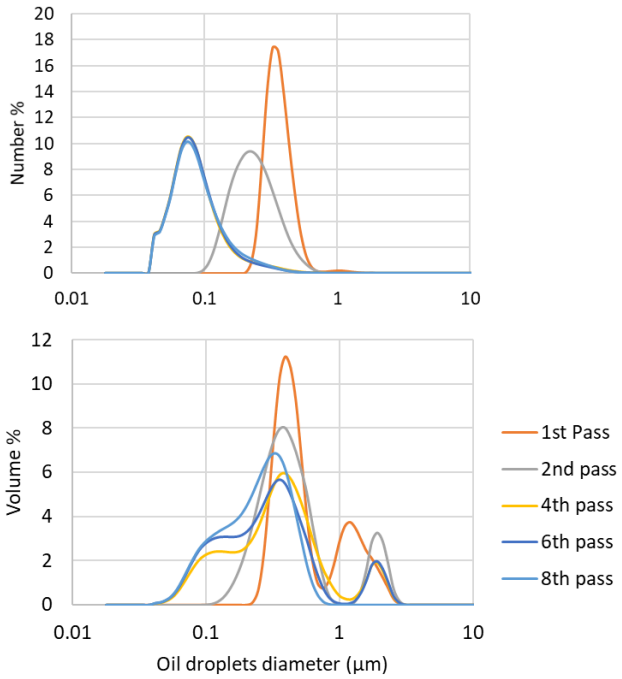

Figure 15: Droplet size distribution of nano-emulsions produced using 1 - 8 emulsification passes, at oil/water volume ratio of 1/500 and emulsification pressure of 1,900 bar

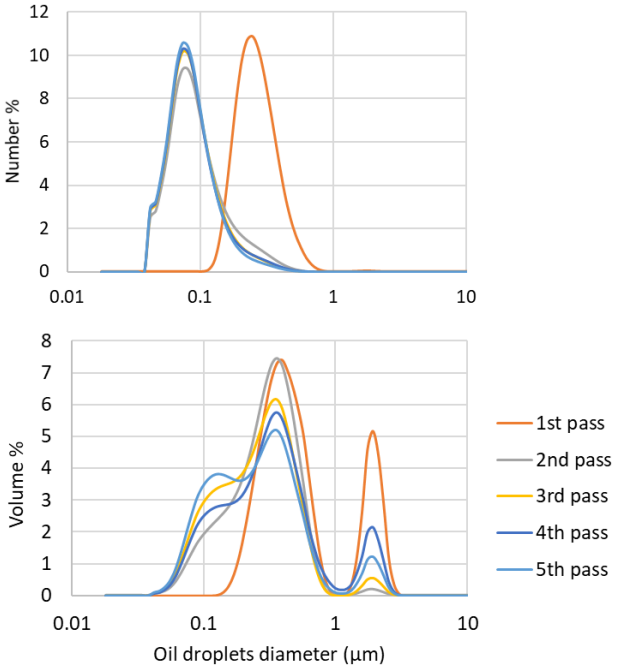

Figure 16: Droplet size distribution of nano-emulsions produced with 1-5 emulsification passes, at oil/water volume ratio of 1/1,000 Oil/Water, and emulsification pressure 1,900 bar

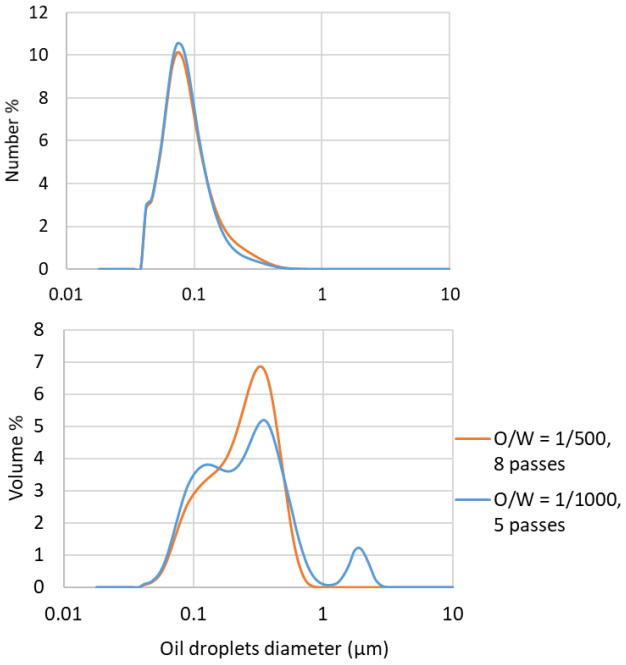

Figure 17: Droplet size distribution of 1/1,000 Oil/Water nano-emulsion produced with five emulsification passes and droplet size distribution of 1/500 Oil/Water nano-emulsion produced with eight emulsification passes

In conclusion, according to the outputs of the previously explained adaptation experiments, three sets of parameters were preferentially chosen to produce three nanoemulsions to be employed in this study, as shown in **Table 5**. **Figure 18** presents the droplet size distribution of the adapted nanoemulsions.

Table 5: Adapted nanoemulsions and the operating conditions

Emulsion	d_{32} (nm)	O/W	Pressure (bar)	Number of Passes
E1	150 – 250	1/1000	1,700	4
E2	350 – 450	1/500	1,700	2
E3	~ 1,000	1/500	1,000	1

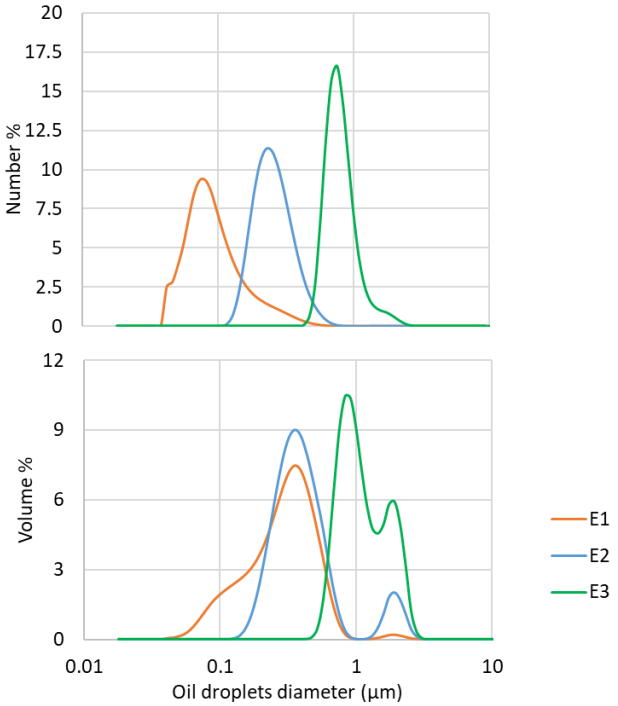

Figure 18: The droplet size distribution for the adapted nanoemulsions

These nano-emulsions were quite reproducible, as indicated in **Figure 19** and **Figure 20** for E1 and E2, respectively**.**

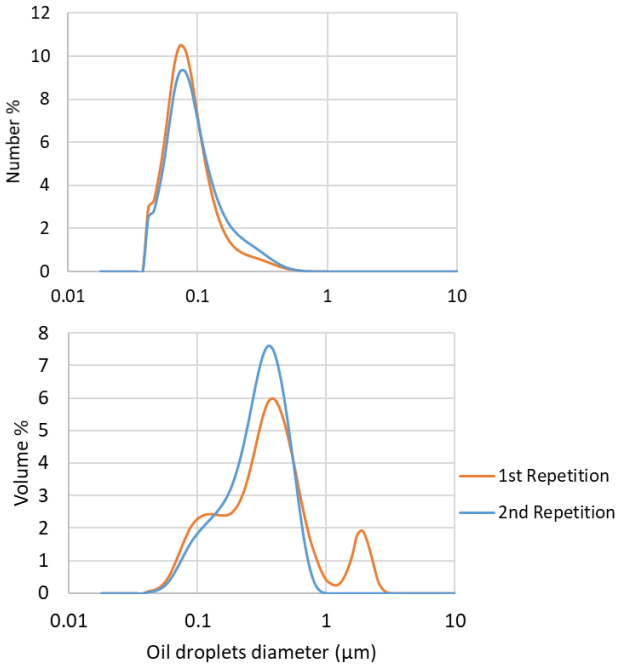

Figure 19: Droplet size distribution of nano-emulsion ($E1_{d32=250}$) and its reproducibility. E1: 1/1,000 oil/water, 1,700 bar and 4 passes

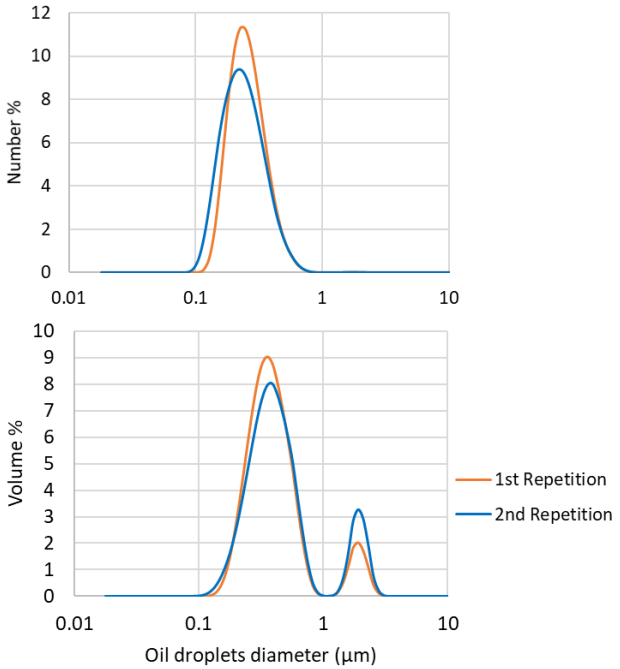

Figure 20: Droplet size distribution of nano-emulsion ($E2_{d32=450}$) and its reproducibility E2: 1/500 oil/water, 1,700 bar and 2 passes

The stability of the produced nano-emulsions was also investigated. As indicated in **Figure 21**, they were found to be stable at least for 24 h. However, it was decided to always use freshly prepared oil emulsions in the filtration experiments to minimize the unforeseen experimental errors.

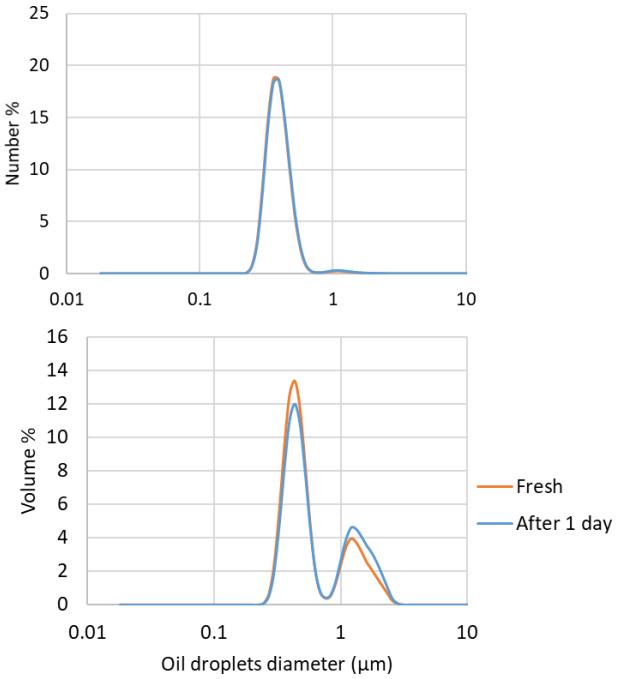

Figure 21: Droplet size distribution of fresh and stored (24 h) E2 nano-emulsion. E2: 1/500 oil/water, 1,700 bar and 2 passes

5.3.2 Fouling behavior of polymeric membranes at constant flux experiments

Three oily feeds, i.e. E1, E2 and E3 were filtered through ceramic and PES membranes S800 (MF, 800 nm), S450 (MF, 450 nm), S100 (MF, 100 nm) and IG (UF, 20 nm) (cf. **5.1.3**). In general, a strong relationship was observed between membranes' fouling behavior and average oil droplet size distribution. Permeability decline curves for filtration experiments using E1, E2 and E3 through MF PES membranes, are shown in **Figure 22 A** and **B**. Besides, the respective fouling mechanisms are indicated in **Figure 23 A** and **B**. In which it is noticed that E1 and E2 feeds caused higher permeability decline than in case of E3, that might be explained by strong internal membrane fouling because of the low average oil droplet size in case of E1 and E2 compared to membranes' pore diameters. Moreover, the chronological analysis of fouling mechanisms indicated that more than 90% of the

decay in MF membrane performance during filtration of E1 and E2 was caused by pore blocking, i.e. intermediate and standard pore blocking.

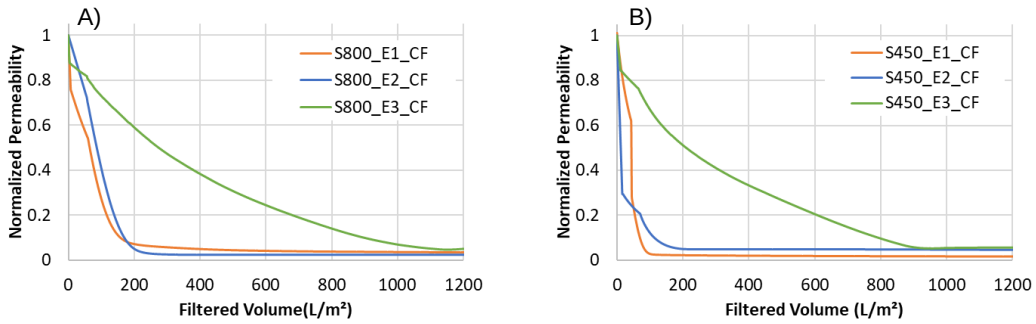

Figure 22: Normalized permeability decline for PES MF membranes, S800 (a) and S450 (b), during filtration of oily feed water prepared from E1, E2 and E3 nano-emulsions at constant flux of 1,300 LMH (one time measurement)

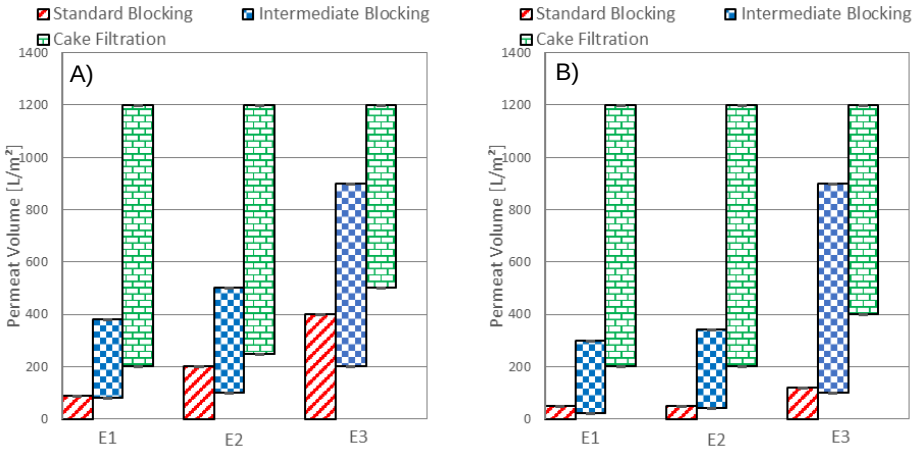

Figure 23: Fouling chronological evolution during the filtration of E1, E2 and E3 using MF membranes S800 (a) and S450 (b) at constant flux of 1,300 LMH (one time measurement)

Nevertheless, in case of UF membranes, i.e. S100 and IG, Permeability decline curves for filtration experiments using E1, E2 and E3 through UF PES membranes (**cf. Figure 24 A** and **B**) and the respective fouling mechanisms (**cf. Figure 25 A** and **B**) indicated that only E1 caused severe decline in membranes' permeability than in cases of E2 and E3, which supports certainly the hypothesis that feed solutions containing oil droplets smaller than / comparable to membranes' pore diameters might lead to substantial decay in membrane performance due to severe internal membrane fouling.

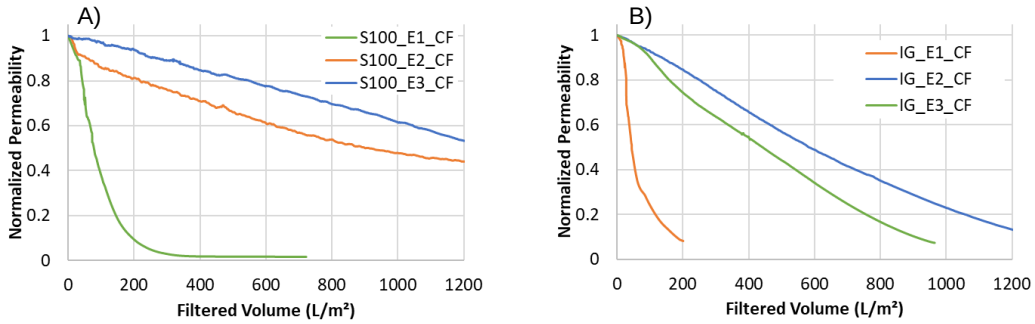

Figure 24: Normalized permeability decline for PES UF membranes, S100 (a) and IG (b), during filtration of oily feed water prepared from E1, E2 and E3 nano-emulsions at constant flux of 240 LMH

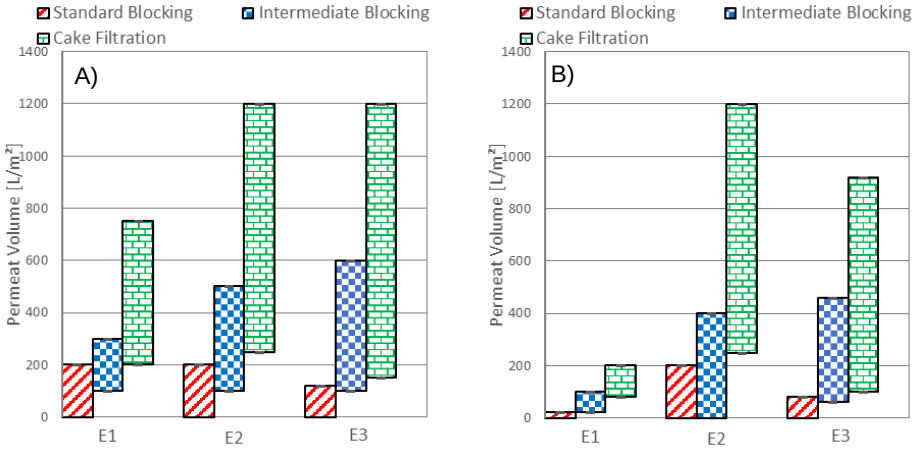

Figure 25: Fouling chronological evolution during the filtration of E1, E2 and E3 using UF membranes S100 (a) and IG (b) at constant flux of 240 LMH

To ensure the reproducibility of the filtration experiments, those with S450 membranes were repeated once again employing E1 and E2 as indicated in **Figure 26** and two other times with E3 as illustrated in **Figure 27,** results showed quite reproducible behaviors during filtration. Furthermore, Experiments at constant pressure using E2 through IG membranes and E1, E2 and E3 through S450 Membranes as well as S100 were repeated once again, and were mostly reproducible (cf. **Appendix**).

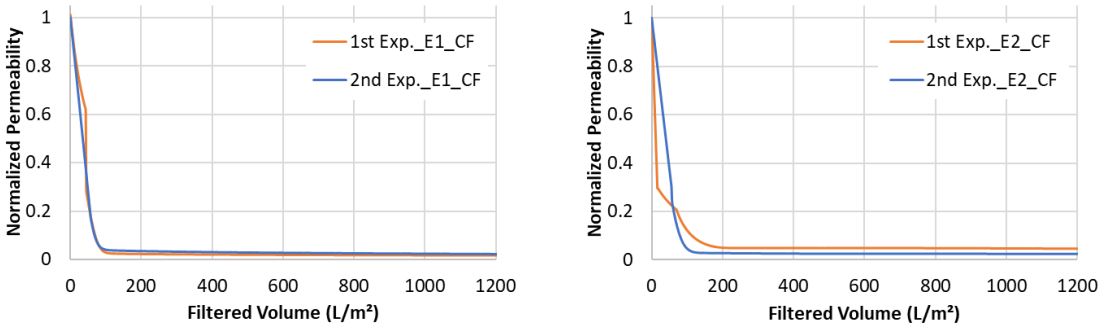

Figure 26: Reproducibility of filtration experiments of E1 and E2 through S450 membranes (Two times measurements)

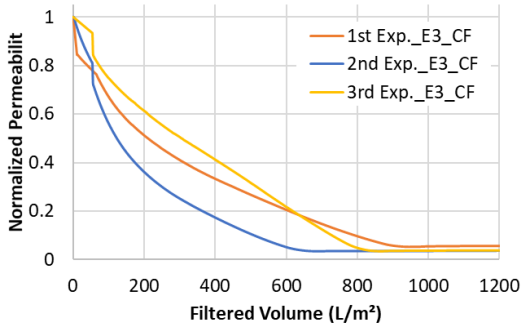

Figure 27: Reproducibility of filtration experiments of E3 through S450 membranes (three times measurements)

5.3.2.1 Membrane morphology

The cross-sectional morphology of exemplary fouled MF membranes, S450, during filtration of three oil feed solutions were analyzed and compared with pristine unfouled membranes. SEM micrograph for virgin S450 membrane (**cf. Figure 28**) showed that membrane exhibited a sponge-like isotropic structure without an active layer.

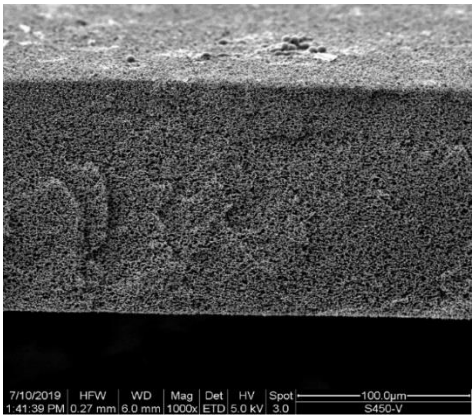

Figure 28: SEM micrograph for virgin S450 (450 nm) membrane, Magnification: X 1000

In addition, SEM micrographs at higher magnification for virgin and fouled S450 membranes, after filtration of E1, E2 and E3 feeds at oil content of 5 mg/L and constant flow rate, are shown in **Figure 29**.

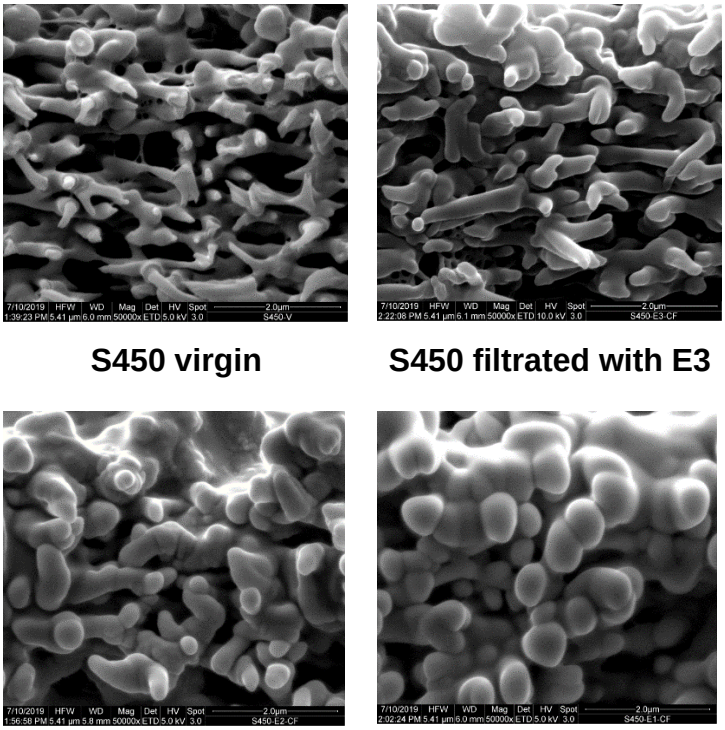

S450 virgin **S450 filtrated with E3**

S450 filtrated with E2 **S450 filtrated with E1**

Figure 29: SEM micrographs for virgin and fouled S450 membranes during filtration of E1, E2 and E3 feed solutions, Magnification: X 50,000

Interestingly membrane fouling was found to be associated with coating of membrane internal fiber structure by oil droplets causing proceeding contraction of internal pores, as can be seen in **Figure 29**. However, the extent of oil incorporation into membrane structures is influenced by different oil droplet size distribution. Very limited oil coating was observed for membranes fouled after filtration of E3 having larger oil droplet sizes. However, in case of E2, more coating of membrane internal structure than E3 was found. Moreover, most severe fouling / intense oil incorporation was observed for fouled membranes by E1, which has small oil droplet size. This supports well the earlier findings regarding the substantial influence of oil droplet size distribution and membrane average pore diameter on the membrane performance and fouling behavior.

5.3.3 *Fouling behavior of polymeric membranes at 0.5 bar constant pressure experiments*

In parallel, filtration experiments using three oil nano-emulsions were also conducted at 0.5 bar constant pressure condition. E1, E2 and E3 feeds were filtered through S800, S450, S100 and IG membranes at constant operation pressure of 0.5 bar. The membrane performance curves and fouling mechanism of MF membranes are introduced in **Figure 30** and **Figure 31**, respectively. In which, E1 and E2 caused stronger permeability decline than E3, which is similar to what was noticed in constant flux experiments.

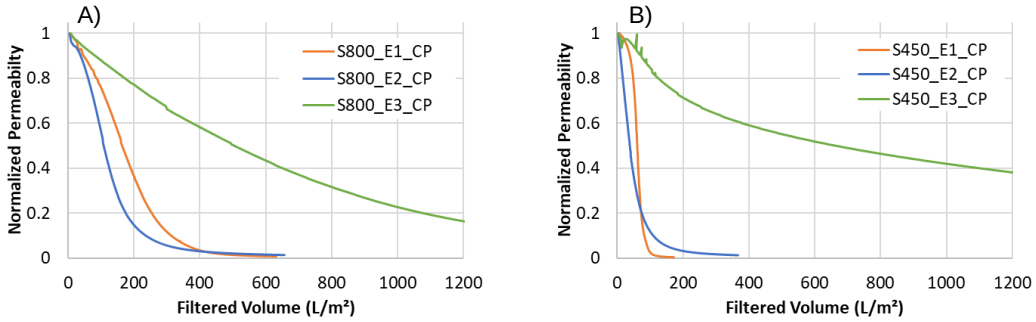

Figure 30: Normalized permeability decline for PES MF membranes, S800 (a) and S450 (b), during filtration of oily feed water prepared from E1, E2 and E3 nano-emulsions at 0.5 bar constant pressure

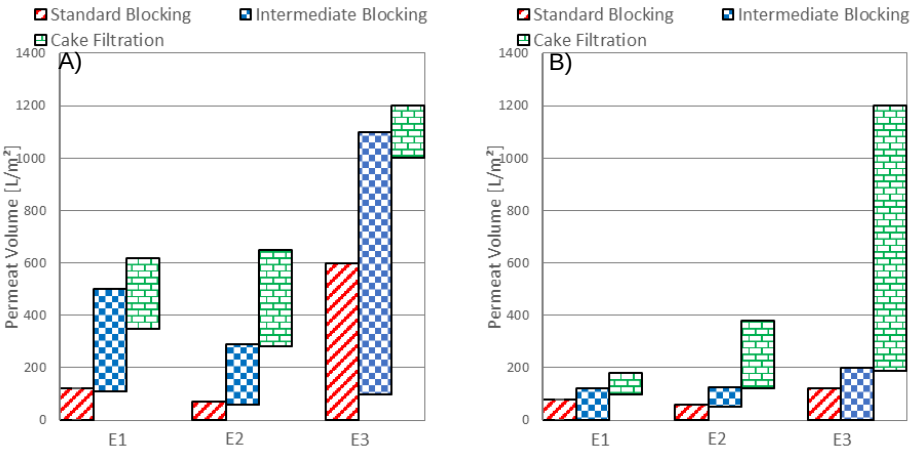

Figure 31: Fouling chronological evolution during the filtration of E1, E2 and E3 using MF membranes S800 (a) and S450 (b) at 0.5 bar constant pressure

Interestingly, in case of UF membranes, as indicated in **Figure 32** and **Figure 33**, which represent . membrane permeability decline curves and the respective fouling mechanism for S100 and IG membranes, E1 and E2 also caused more decay in

membrane performance than E3. E2 was expected to cause fouling behavior comparable to E3 since they both contain oil droplets that are bigger than pores of UF membranes. This effect might be explained by considering that oil droplets are directly subject to a high constant pressure from the beginning which might push the drops into the pores causing high fouling rate. Whereas, in case of constant flux, they can lay at the membrane with low pressure at the initial conditions under constant flow rate to prevent following drops from penetrating through the pores.

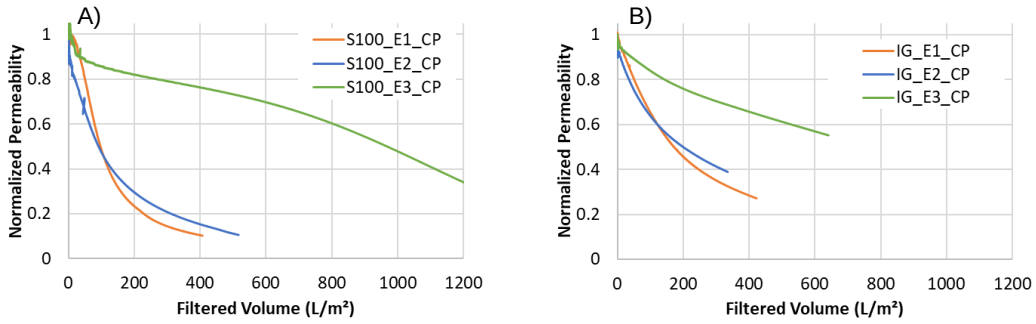

Figure 32: Normalized permeability decline for PES UF membranes, S100 (a) and IG (b), during filtration of oily feed water prepared from E1, E2 and E3 nano-emulsions at 0.5 bar constant pressure.

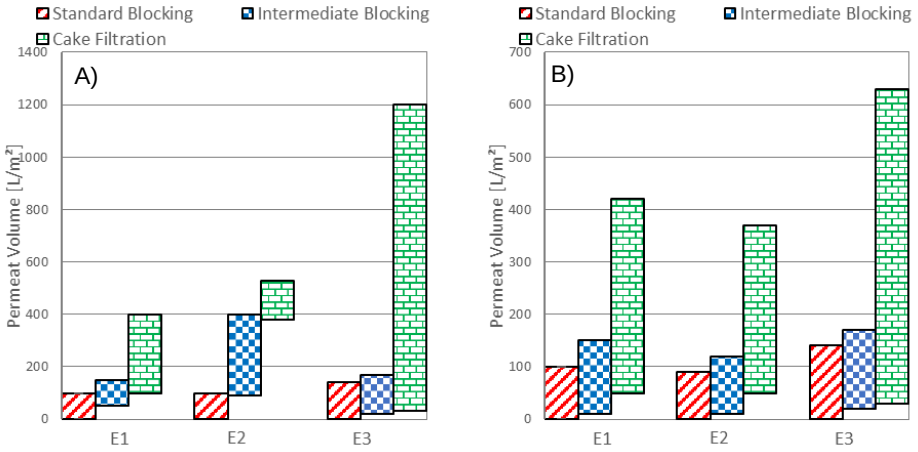

Figure 33: Fouling chronological evolution during the filtration of E1, E2 and E3 using MF membranes S800 (a) and S450 (b) at 0.5 bar constant pressure

5.3.4 *Fouling behavior of polymeric membranes at 2.07 bar constant pressure experiments*

At the early stages of the work, a set of preliminary filtration experiments were carried out at 2.07 bar constant pressure conditions. The main target of these experiments was to check the significance of the droplet size influence on the fouling

behavior as well as to adjust the experimental conditions. In this group of experiments PES membranes 4F (400 nm), 1F (100 nm) and IG (20 nm) were employed. It is also of interest to mention that nano-emulsions of those experiments were not subject of the fining step, i.e. final filtration step to remove droplets >10 µm, so they might contained some extra big drops that were not detect by the size measurement (cf. 5.2.4). However, results emphasized the significant influence of the oil droplet size along with the membrane average pore diameter on the fouling behavior, and consequently on fouling mechanisms. Such influence was found to be more pronounced in case of MF membranes rather than UF membranes. For instance, the permeability decline curves of 4F, 1F and IG PES membranes (cf. **Figure 34, Figure 35** and **Figure 36**, respectively) showed different fouling behavior during the filtration of E1* and E2* nano-emulsions. As illustrated in **Figure 34** for 4F membranes, E1* nano-emulsions caused higher permeability decline than E2* nano-emulsions. In parallel, application of pore blocking filtration models (see **Figure 37**) to fouling curves of 4F membranes showed that intermediate pore blocking was the dominant fouling mechanism during filtration of E2*, while in case of E1*, severe standard pore blocking followed by intermediate blocking and then cake filtration were found.

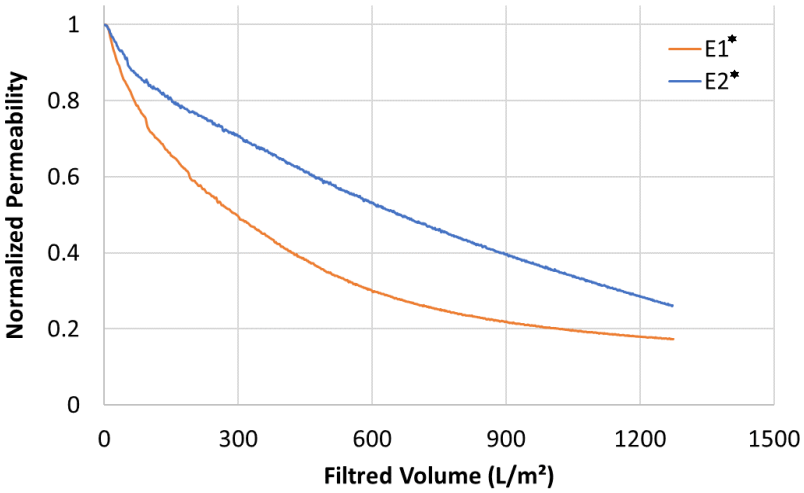

Figure 34: Normalized permeability decline of 4F (400 nm) membranes when filtering oily feed waters prepared from E1* and E2* nano-emulsions (average of two measurements)

On the other hand, as depicted in **Figure 36,** similar fouling behavior compared to 1F membrane could be noticed in case of IG membranes. Only slight difference

can be noticed between permeability decline curves of 1F and IG membranes, in which 1F membranes experienced stronger fouling during the early phase of filtration, even though they showed comparable chronological development of fouling mechanisms.

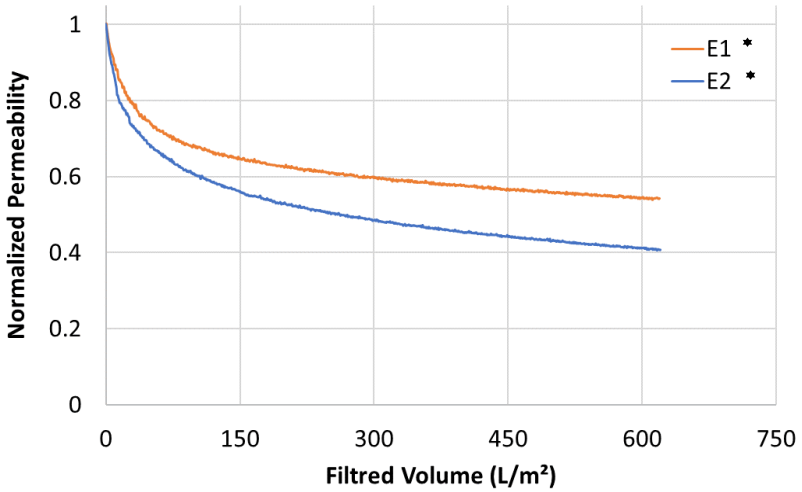

Figure 35 : Normalized permeability decline of 1F (40 nm) membranes when filtering oily feed waters prepared from E1* and E2* nano-emulsions (average of two measurements)

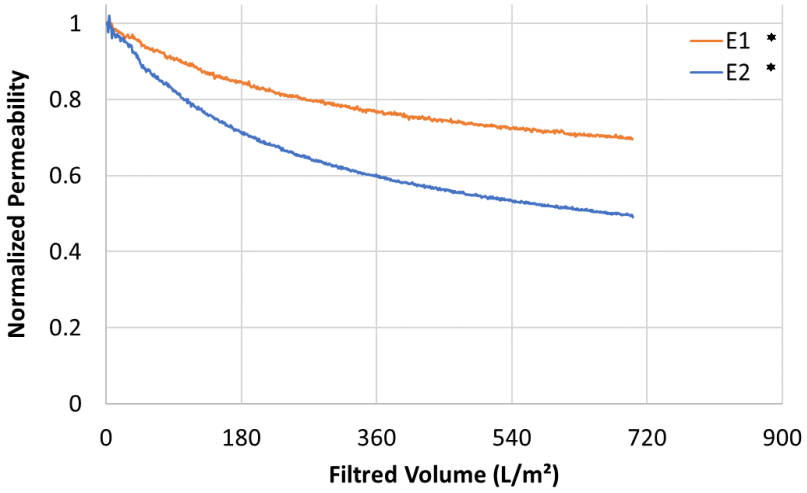

Figure 36: Normalized permeability decline of IG (20 nm) membranes when filtering oily feed waters prepared from E1* and E2* nano-emulsions (average of two measurements).

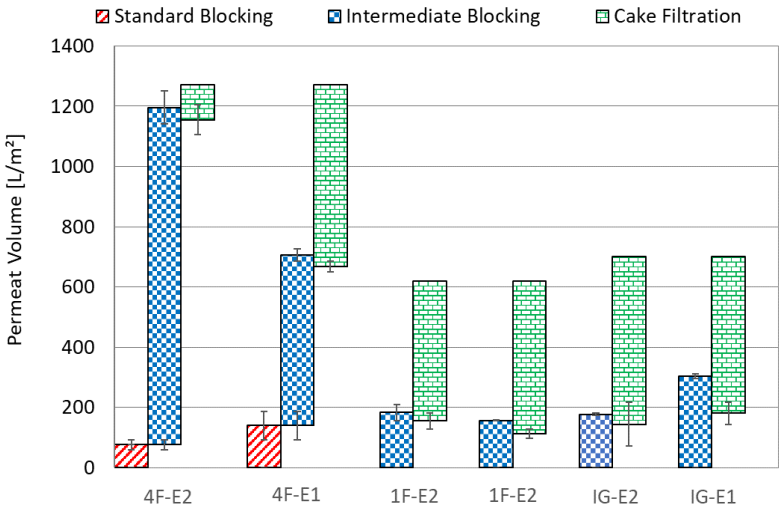

Figure 37: Fouling chronological evolution during the filtration of E1* and E2* using 4F (400 nm), 1F (40 nm) and IG (20 nm) membranes (average of two measurements)

Furthermore, morphological studies for the virgin and fouled PES membranes were conducted using SEM and ESEM, respectively. The cross section SEM analysis of 4F membranes (cf. **Figure 38**) showed that the oil droplets could go into the membrane pores and fill the internal voids causing severe internal fouling in addition to surface fouling. However, no oil was observed in the internal structure of IG PES membranes.

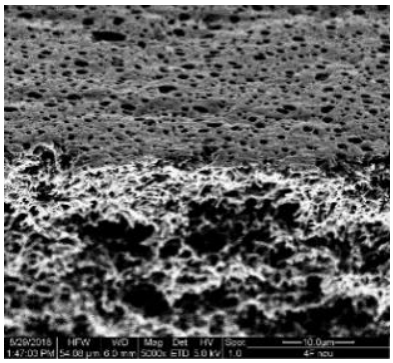

4F virgin
Magnification: X 5,000

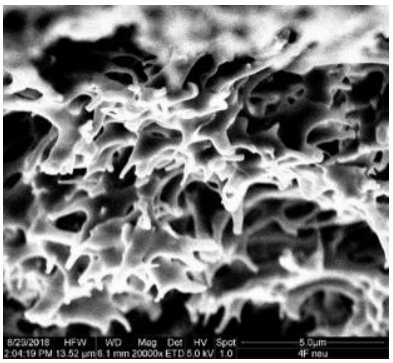

4F virgin, the cross section
Magnification: X 20,000

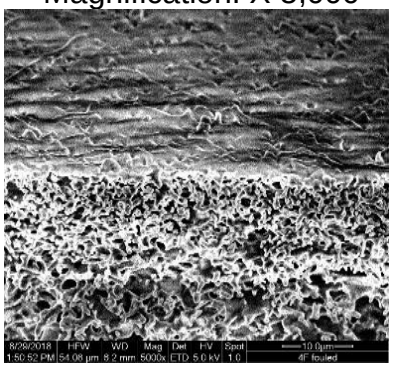

4F Fouled
Magnification: X 5,000

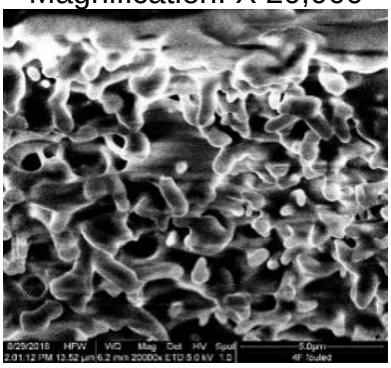

4F fouled, cross section
Magnification: X 20,000

Figure 38: SEM micrographs for virgin (and fouled 4F (400 nm) membranes after filtration of 5 mg/L of E2* nano-emulsion

Furthermore, ESEM micrographs of IG, 4F and 1F membranes (cf. **Figure 39)** showed that the deposited oil droplets formed a kind of continuous oil film atop IG membranes when a layer that contains discriminate oil droplets was noticed on top of 4F and 1F membranes.

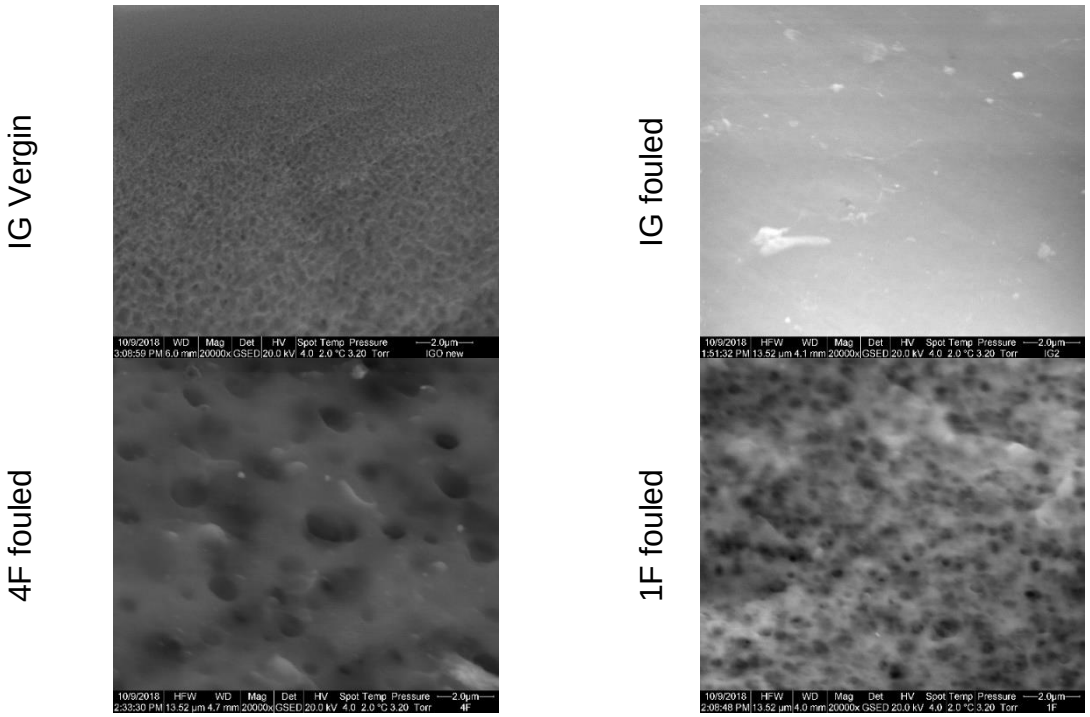

Figure 39: ESEM micrographs of the surface of IG, 4F and 1F after filtering 5 mg/L of E2* nanoemulsion

5.3.5 *Fouling behavior of ceramic membranes at constant pressure experiments*

Filtration experiments using ceramic membranes has generally revealed the hypotheses made out experiments with polymeric membranes. In which, droplets in the same size as the membrane pores caused severe fouling and constant pressure conditions caused more permeability decline than constant flux conditions as indicated in **Figure 40** and **Figure 41** which shows the permeability decline curves and the correspondent blocking mechanisms, respectively, when comparing the filtration behavior of E2* through TM 045 (450 nm) at constant pressure and constant flux.

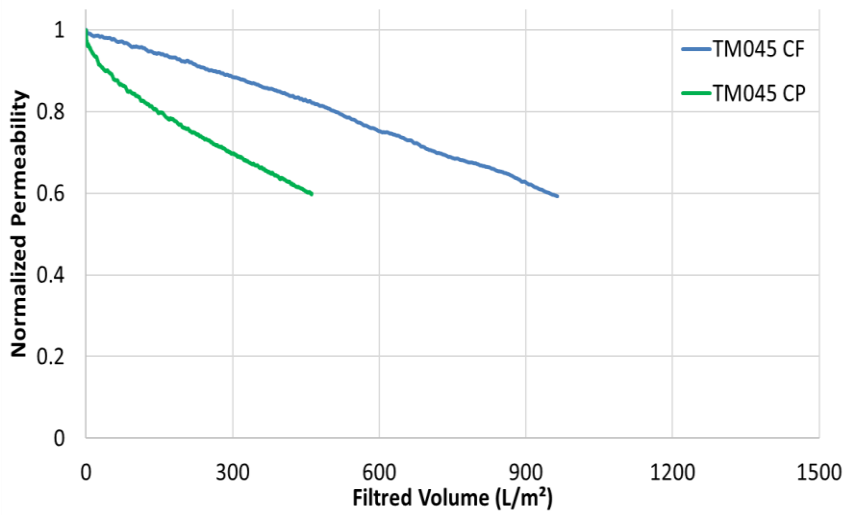

Figure 40: Normalized permeability decline of TM045 (450 nm) membranes when filtering oily feed waters prepared from E2* nano-emulsions under 2.07 bar constant pressure (CP) and 240 L/m².h constant flow rate (CF)

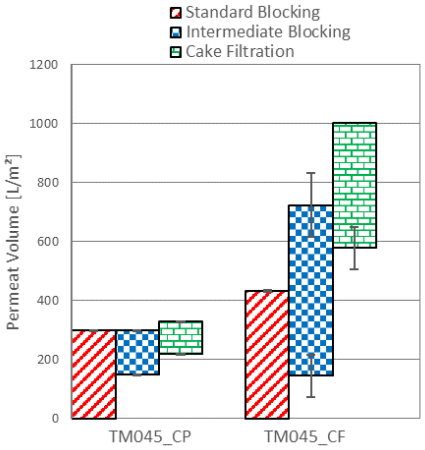

Figure 41: Fouling chronological evolution during the filtration of E2* using TM045 (450 nm) at constant pressure (CP) and constant flow rate (CF)

As depicted in **Figure 42,** permeability decline curves during filtration of E2 nano-emulsions through membranes with pores of much smaller than the oil droplets like TU015 (15 kDa) and TU050 (50 kDa) ceramic membranes, showed quite similar membrane fouling behavior, in which cake filtration model was dominating the fouling mechanism, as revealed from **Figure 43.**

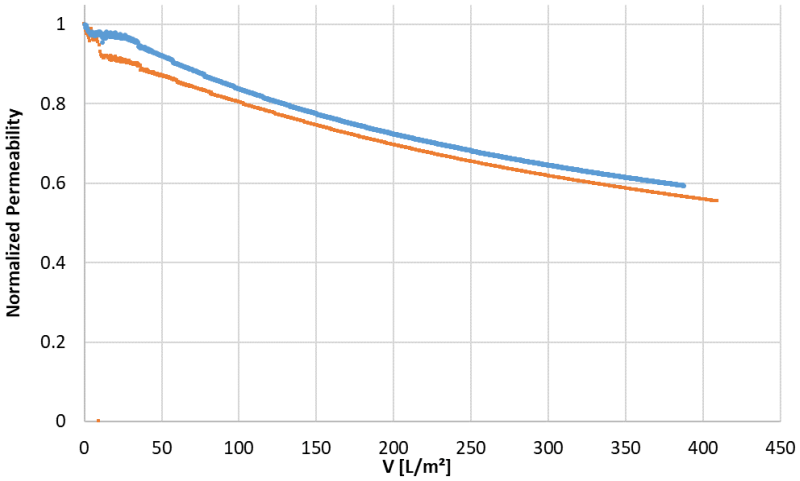

Figure 42: **Normalized permeability decline of oily feed waters prepared from E1* (orange) and E2*(blue) nano-emulsions for TU015 (15 kDa) and TU050 (50 kDa) membranes**

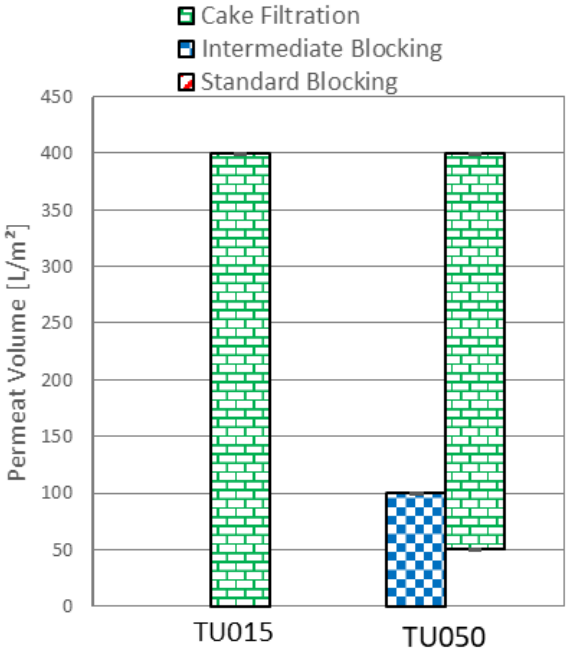

Figure 43: **Fouling chronological evolution during the filtration of E2* using TU015 (15 kDa) and TU050 (50 kDa)**

5.3.6 Influence of salt content on the filtration behavior

A set of experiments was carried out for testing the influence of different salt content in oily feed's background water by filtering oily feeds prepared of E1 nano-emulsions with no salt, 0.5 M NaCl, 0.5 M $CaCl_2$, a mix of 0.5 M NaCl and $CaCl_2$, 1 M NaCl as well as artificial seawater salt solution (ASW) through S100 and S450 membranes. Furthermore, oil droplets size distribution was measured before and after adding salts. Results revealed that salts mainly influence the stability of the oily feed, i.e., formation of larger drops has been noticed as shown in **Figure 44**.

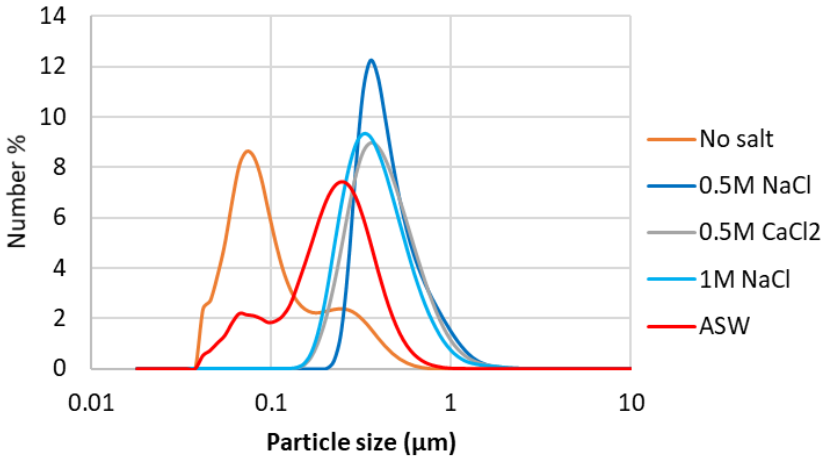

Figure 44: Droplet size distribution of oily feeds prepared of E1 nano-emulsions with no salt, 0.5 M NaCl, 0.5 M $CaCl_2$, 1 M NaCl and artificial sea water salts (ASW)

Conductivity and Zeta potential of oily feeds are shown in **Table 6.** All feeds are negatively charged and salt addition has decreased the absolute zeta potential.

Table 6: Conductivity and Zeta potential of oily feeds prepared of E1 nano-emulsions with no salt, 0.5 M NaCl, 0.5 M $CaCl_2$, mix of 0.5 NaCl and $CaCl_2$, 1 M NaCl and artificial sea water salts (ASW)

Sample	Conductivity in µS/cm	Zeta Potential in mV
E1 – No Salt	60	- 45
E1 – 0.5 M NaCl	46,160	- 23,3
E1 – 0.5 M $CaCl_2$	76,200	- 1.3
E1 – 0.5 M Mix	112,500	- 1.4
E1 – 1 M NaCl	92,600	- 15.4
E1 – ASW	50,400	- 7.3

The permeability decline curves of E1 oily feed filtered through S450 and S100 at constant flux of 240 and 1300 LMH, as depicted in **Figure 45** and **Figure 46**, respectively. The fouling behavior of nano-emulsions through both membranes was previously addressed (cf. 5.3.2), in which a strong permeability decline for both membranes and the fouling behavior was comparable for both membranes, in which they lost 90% of their permeability after filtering about 200 and 100 L/m² for S450 and S100, respectively.

However, adding salt led to enhance the S450 membrane performance (cf. **Figure 45**), i.e., less permeability decease was noticed. In which the 90% permeability loss occurred after filtering about 350, 500, 550 and 650 L/m² for 0.5 M $CaCl_2$, 0.5 M mix, ASW and 0.5 M NaCl, respectively.

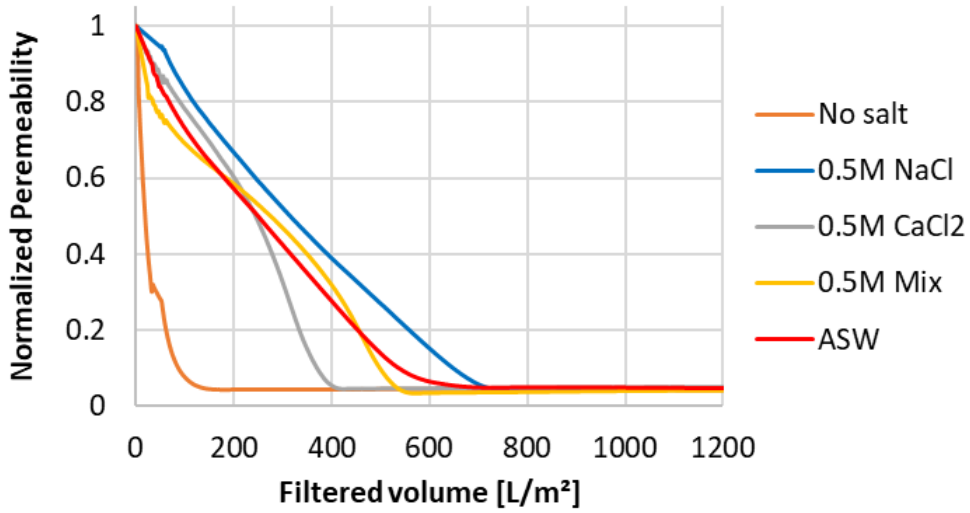

Figure 45: Normalized permeability decline of oily feeds prepared of E1 nano-emulsions with no salt, 0.5 M NaCl, 0.5 M $CaCl_2$, mix of 0.5 M NaCl and $CaCl_2$, 1 M NaCl and artificial seawater salts (ASW) filtered through S450 membranes

In the other hand, salts led to more significant enhancement in the performance of S100 membranes, in which ASW was found to cause the lowest permeability decline of only about 10% after filtering 1200 L/m², at which membranes were almost blocked when other oily feeds were employed.

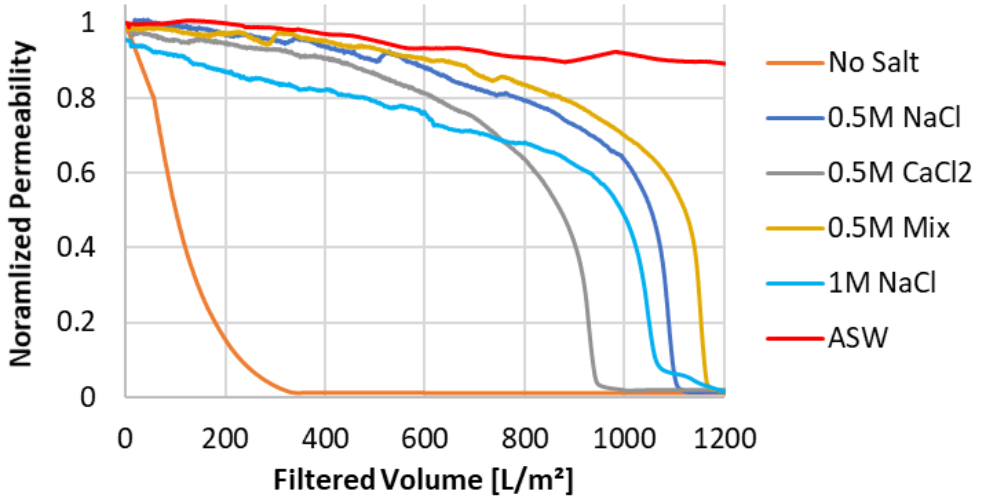

Figure 46: Normalized permeability decline of oily feeds prepared of E1 nano-emulsions with no salt, 0.5 M NaCl, 0.5 M $CaCl_2$, mix of 0.5 M NaCl and $CaCl_2$, 1 M NaCl and artificial seawater salts (ASW) filtered through S100 membranes

5.3.7 Feasibility of membrane cleaning

To investigate the feasibility of membrane cleaning and to find out the most effective cleaning agents, several cleaning tests were performed. Cleaning experiments included testing of acetic acid, NaOH, NaOCl (200 ppm free chlorine) and a combination of NaOH followed by acetic acid at different pH values as illustrated in **Table 7**.

Table 7 List of tested cleaners and their efficiency by restoring the pre-experiment pure water permeability

Cleaner	PH	Recovery %
NaOCl	12.5	92.5
NaOH → Acetic Acid	12 →2	92
NaOH	12	85
Acetic acid	2	59

Afterwards, all membranes were cleaned with NaOCl again, and the cleaning tests were carried out again using NaOH at pH = 12 with boiling for 60 min, at pH ≈ 14 with heating for 5 and 60 min, which could recover 95, 97 and 98% of the pre-experiment permeability. That indicate that heating could improve cleaning process but none of the procedures could recover the initial permeability of the virgin membrane

5.4 Conclusion

W-UFO I has studied the influence of oil droplet size distribution, membrane barrier pore size on the membrane fouling behavior and separation performance. Besides, the chronological development of fouling mechanisms for UF and MF membranes were explored. Membrane fouling mechanisms were properly interpreted using pore blocking filtration models. Moreover, the influence of salts on the stability of oil droplets in feed solutions has been investigated. The main scientific outputs are summarized in the following points:

- UF and MF membranes' performance and nature of fouling mechanisms were emphasized to be substantially influenced by the interrelation between oil droplet size distribution and membrane pore size distribution.
- In case of the used MF membranes (pore size larger than droplet size of oily emulsions), fouling mechanisms were dominated by standard pore blocking at early stage of filtration, afterward, more contribution of intermediate blocking and cake filtration mechanisms were observed. This indicates that severe decay in MF membranes' performance should be mainly related to internal membrane fouling. This conclusion was additionally supported by SEM analysis of fouled MF membranes, where oil droplets were seen to penetrate and coating the internal membrane structure.
- In case of the used UF membranes (pore size smaller than droplet size of oily emulsions), fouling mechanisms were rather prevailed by intermediate and cake filtration fouling models, which means that fouling of more dense membranes by produced water should be interpreted in terms of surface fouling rather than internal pore blocking if pore size is sufficiently small.
- Accordingly, it is highly recommended to analyze oily feeds in terms of droplet size distribution to choose the most suitable membrane, i.e., the one with pores smaller than oil droplets, to avoid harmful internal fouling.
- The influence of operating / filtration parameters on membranes' performance was also studied. Briefly, performing experiments at high initial pressure in case of constant pressure experiments have led to intensive internal fouling and severe decay in membrane performance. In contrast increasing

TMP at later filtration periods was observed to have less detrimental impact on membrane performance, as in case of constant flux experiments.

- Addition of salts was found to disturbs the stability of oil nano-emulsions and resulting in bigger oil droplets, and consequently, oil droplet size distributions with bigger droplets are highly expected in case of real saline produced water. Subsequently, saline oily feeds caused less membrane fouling.
- The cleaning protocol, i.e., rinsing in NaOH at pH=14 and 100 °C for 60 min, was found to be able to restore 98 % of the membrane pre-experiment permeability. But none of the tested cleaning protocols could restore the permeability of virgin membrane.

6 Outlook

Based on the results of W-UFO-I in the next phase of total W-UFO project, a number of topics should be investigated detailed.

- The individual and combined influences of salts, surfactants and co-surfactants on the stability and droplet size distribution of oil nano-emulsions, and consequently, on membrane performance as well as on fouling mechanisms.
- The maximum critical pressure, as well as the maximum flow rate, that can be applied without causing initial severe fouling to reduce fouling. Such parameters will be addressed in future work for the optimization of operational conditions (planned in W-UFO-IV).

7 References

1. Liang, Y., et al., *Chapter Fourteen - Special Focus on Produced Water in Oil and Gas Fields: Origin, Management, and Reinjection Practice*, in *Formation Damage During Improved Oil Recovery*, B. Yuan and D.A. Wood, Editors. 2018, Gulf Professional Publishing. p. 515-586.
2. Ray, J.P. and F.R. Engelhardt, *PRODUCED WATER, Technological/Environmental Issues and Solutions.* 1992.
3. Ahmadun, F.l.-R., et al., *Review of technologies for oil and gas produced water treatment.* Journal of Hazardous Materials, 2009. **170**(2): p. 530-551.

4. Jiménez, S., et al., *State of the art of produced water treatment.* Chemosphere, 2018. **192**: p. 186-208.

5. Røe Utvik, T.I., *Chemical characterisation of produced water from four offshore oil production platforms in the North Sea.* Chemosphere, 1999. **39**(15): p. 2593-2606.

6. Neff, J., K. Lee, and E. Deblois, *Produced Water: Overview of Composition, Fates, and Effects*. 2011. p. 3-54.

7. Igunnu, E.T. and G.Z. Chen, *Produced water treatment technologies.* International Journal of Low-Carbon Technologies, 2014. **9**(3): p. 157-177.

8. Duraisamy, R.T., A.H. Beni, and A. Henni, *State of the Art Treatment of Produced Water*, in *Water Treatment*, W. Elshorbagy and R.K. Chowdhury, Editors. 2013, InTech: Rijeka. p. Ch. 09.

9. Bilstad, T. and E. Espedal, *Membrane separation of produced water.* Water Science and Technology, 1996. **34**(9): p. 239.

10. Yu, L., M. Han, and F. He, *A review of treating oily wastewater.* Arabian Journal of Chemistry, 2017. **10**: p. S1913-S1922.

11. Je, Y., *Membrane technologies for water treatment and reuse in the gas and petrochemical industries*, in *Advances in membrane technologies for water treatment : materials, processes and applications*, A. Basile, A. Cassano, and N.K. Rastogi, Editors. 2015, Elsevier, Woodhead Publishing: Amsterdam.

12. Funk, W., V. Dammann, and G. Donnevert, *Qualitätssicherung in der analytischen chemie: anwendungen in der umwelt-, lebensmittel-und werkstoffanalytik, biotechnologie und medizintechnik*. 2005: John Wiley & Sons.

13. Iritani, E. and N. Katagiri, *Developments of Blocking Filtration Model in Membrane Filtration.* KONA Powder and Particle Journal, 2016. **33**: p. 179-202.

14. Hermans, P.H. and H.L. Bredée, *Zur Kenntnis der Filtrationsgesetze.* Recueil des Travaux Chimiques des Pays-Bas, 1935. **54**(9): p. 680-700.

15. Hermans, P. and H.L. Bredée, *Principles of the mathematical treatment of constant-pressure filtration.* J. Soc. Chem. Ind., 1936. **55**: p. 1-4.

16. Hermia, J., *Constant pressure blocking filtration law application to powder-law non-Newtonian fluid.* Trans. Inst. Chem. Eng., 1982. **60**: p. 183-187.

17. Huang, H., T.A. Young, and J.G. Jacangelo, *Unified membrane fouling index for low pressure membrane filtration of natural waters:*

principles and methodology. Environmental science & technology, 2007. **42**(3): p. 714-720.

18. Grace, P.H., *Structure and performance of filter media. II. Performance of filter media in liquid service*. Vol. 2. 1956. 316-336.
19. Hlavacek, M. and F. Bouchet, *Constant flowrate blocking laws and an example of their application to dead-end microfiltration of protein solutions.* Journal of Membrane Science, 1993. **82**(3): p. 285-295.
20. Wang, F.L. and V.V. Tarabara, *Pore blocking mechanisms during early stages of membrane fouling by colloids.* Journal of Colloid and Interface Science, 2008. **328**(2): p. 464-469.
21. Xu, W.D. and S. Chellam, *Initial stages of bacterial fouling during dead-end microfiltration.* Environmental Science & Technology, 2005. **39**(17): p. 6470-6476.
22. Yuan, W., A. Kocic, and A.L. Zydney, *Analysis of humic acid fouling during microfiltration using a pore blockage-cake filtration model.* Journal of Membrane Science, 2002. **198**(1): p. 51-62.
23. Suarez, J.A. and J.M. Veza, *Dead-end microfiltration as advanced treatment for wastewater.* Desalination, 2000. **127**(1): p. 47-58.

Appendix

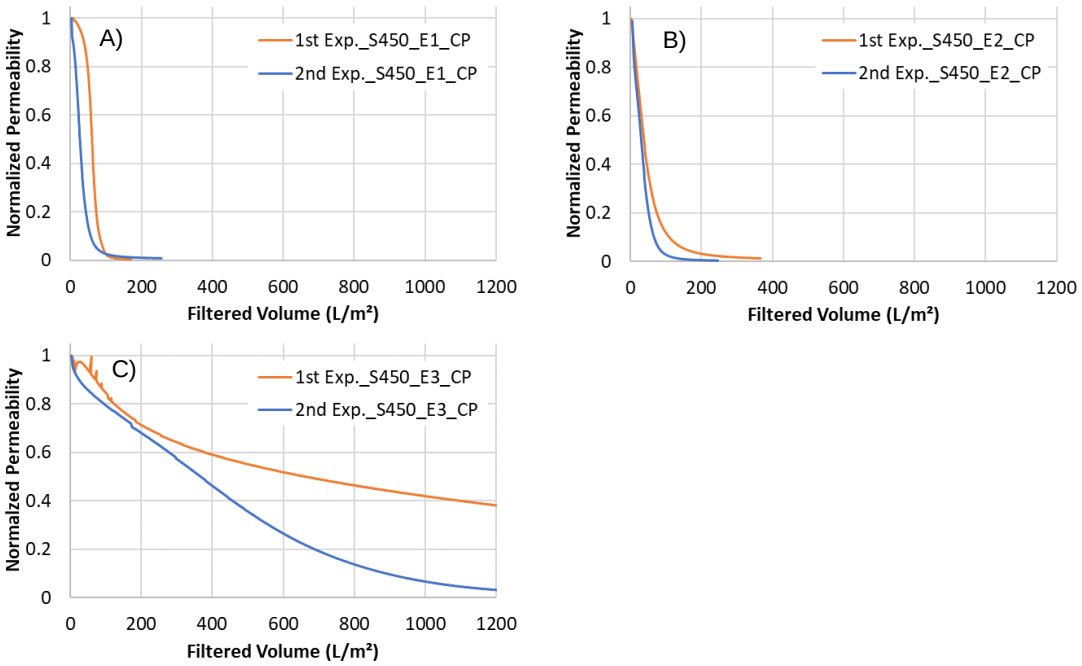

Figure 47: Reproducibility of E1 (a), E2 (b) and E3 (c) by filtration through S450 at 0.5 bar constant pressure

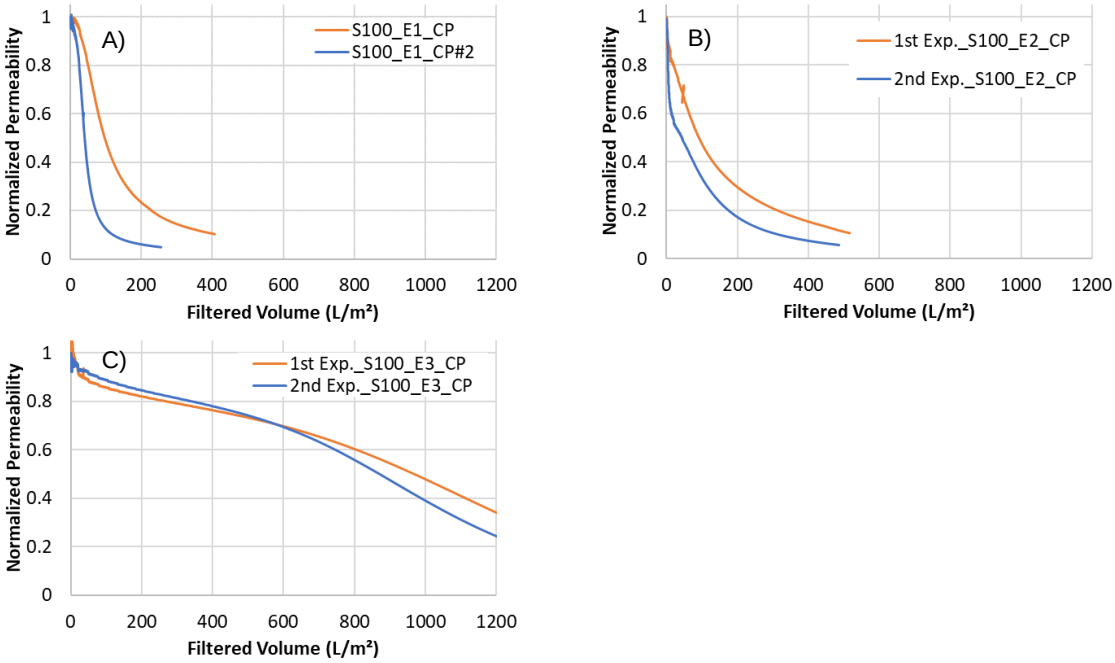

Figure 48: Reproducibility of E1 (a), E2 (b) and E3 (c) by filtration through S100 at 0.5 bar constant pressure

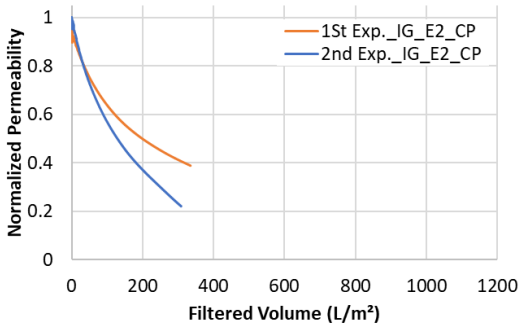

Figure 49: Reproducibility of Filtering E2 through IG and E3 through

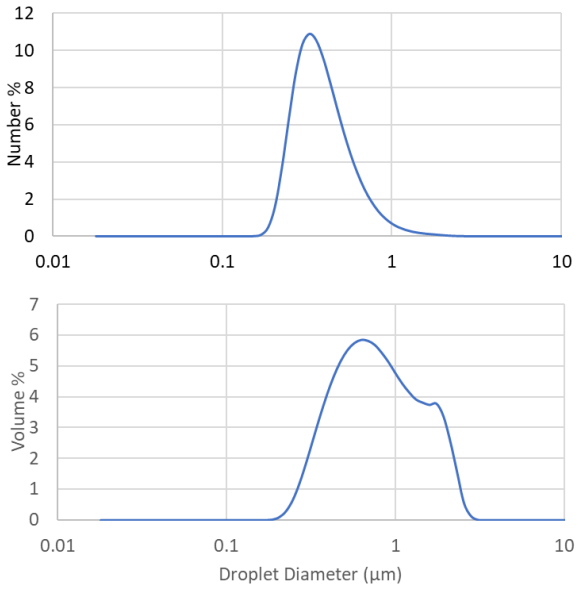

Figure 50: Droplet size distribution of real produced sample from a crude oil and natural gas producer, Germany. The sample was pre-filtered with 10-20 µm qualitative filter